Published in final edited form as:
Nat Cell Biol. 2020 February 01; 22(2): 213–224. doi:10.1038/s41556-019-0456-5.

FERARI is required for Rab11-dependent endocytic recycling

Jachen A. Solinger[#],
Harun-Or Rashid[#],
Cristina Prescianotto-Baschong,
Anne Spang[*]
Biozentrum, University of Basel, Klingelbergstrasse 70, CH-4056 Basel, Switzerland

[#] These authors contributed equally to this work.

Abstract

Endosomal transport is essential for cellular organization and compartmentalization and cell-cell communication. Sorting endosomes provide a crossroad for various trafficking pathways and determine recycling, secretion or degradation of proteins. The organisation of these processes requires membrane tethering factors to coordinate Rab GTPase function with membrane fusion. Here, we report a conserved tethering platform that acts in the Rab11 recycling pathways at sorting endosomes, which we name FERARI (Factor for Endosome Recycling And Rab Interactions). The Rab binding module of FERARI consists of Rab11FIP5/RFIP-2 and rabenosyn-5/RABS-5, while the SNARE interacting module comprises VPS45 and VIPAS39/SPE-39. Unexpectedly, the membrane fission protein EHD1/RME-1 is also a FERARI component. Thus, FERARI appears to combine fusion activity through the SM protein VPS45 with pinching activity through EHD1/RME-1 on SNX-1-positive endosomal membranes. We propose that coordination of fusion and pinching through a kiss-and-run mechanism drives cargo at endosomes into recycling pathways.

Keywords

tether; recycling endosomes; endocytosis; *C. elegans* ; small GTPases; SM protein; SNAREs; vesicle transport; Rab proteins; mammalian cells; recycling; CRISPR; membrane fusion; membrane fission

[*]Corresponding Author: Anne Spang, Biozentrum, University of Basel, Klingelbergstrasse 70, CH-4056 Basel, Switzerland, anne.spang@unibas.ch, Phone: +41 61 207 2380.

Author contributions
JAS, HR and AS conceived and designed the study. JAS, HR and CPB performed the experiments. JAS, HR, CPB and AS analysed and discussed the data. JAS and AS wrote the manuscript with input from all authors.

Competing interest statement
The authors declare no competing interests

Europe PMC Funders Author Manuscripts

Introduction

Endocytosis is essential for the communication of the cell with its environment, controlling cell growth and regulating nutritional uptake. About 70-80% of endocytosed material is recycled back from sorting endosomes to the plasma membrane through different pathways. Defects in recycling lead to a myriad of human diseases such as cancer, ARC (Arthrogryposis–renal dysfunction–cholestasis), BBS (Bardet–Biedl syndrome) or Alzheimer's disease [1–8]. Yet, sorting into recycling endosomes and the interaction of recycling with sorting endosomes remain poorly understood.

The identity of recycling endosomes is largely characterized by the presence of a specific Rab GTPase on the limiting membrane of the organelle. For example, Rab4 and Rab11 are present on different types of recycling endosomes targeted to the plasma membrane. Rab9 is involved in recycling from the sorting endosome to the TGN and Rab10 has multiple reported roles in recycling from endosomes to the TGN or basal lateral membranes and exocytosis from the TGN [9, 10]. The different recycling pathways also highlight a robustness of the system, in that if one recycling pathway is impaired, alternative routes are still available. Yet, it also underscores the difficulty in studying these pathways because of their redundancy.

The number of recycling pathways is reduced in simpler eukaryotes such as *C. elegans*, which lacks Rab9 and Rab4. Yet, *C. elegans* maintains complex organ structures like polarized intestinal epithelia cells, providing an excellent system to analyze recycling processes [11, 12]. In fact, the recycling protein, RME-1, was discovered in *C. elegans* [13]. RME-1 and the homologous human EHD proteins were shown to have tubulation and vesiculation activities [14–16]. EHD1 interacts with Rab11 effectors Rab11FIP2 and Rab11FIP5 and is involved in Rab11-dependent recycling from tubular endosomal networks [17, 18]. The formation of these structures requires BAR domain proteins, most prominently sorting nexins (SNXs). Indeed, SNX4 associates with Rab11 recycling endosomes [19, 20]. In addition, EHD1 interacts with rabenosyn-5 to form recycling compartments [21].

Besides the coordination of recycling pathways, sorting endosomes have to cope with incoming material from the TGN through the biosynthetic route. This cargo has to be sorted into different domains presumably overlapping with recycling pathways. Fusion of transport containers with endosomes is regulated by tethering factors and SNAREs. CORVET and HOPS multisubunit tethering factors have been demonstrated to act on early and late endosomes, respectively [12, 22–25]. The yeast HOPS and CORVET complexes only differ in two subunits, which recognize Rab7/Ypt7 and Rab5/Vps21, respectively [22]. In metazoans, two of the shared HOPS/CORVET components are duplicated. Vps16 has a homolog, VIPAS39/SPE-39 and the Sec1/Munc18 (SM) protein Vps33 is present as Vps33A/VPS-33.1 and Vps33B/VPS-33.2 [24]. Moreover, all eukaryotes contain another SM protein, VPS45, with a proposed function in endosomal recycling [26].

We had speculated recently that VIPAS39/SPE-39 might be part of two HOPS/CORVET types of complexes, one in conjunction with Vps33B/VPS-33.2 and one with VPS45, which we named CHEVI (class C Homologs in Endosome-Vesicle Interaction) and FERARI

(Factors for Endosome Recycling And Retromer Interaction), respectively [27]. Since the nomenclature of retromer is ambiguous, we replaced 'Retromer' for 'Rab' in FERARI. Here, we demonstrate the existence of FERARI in *C. elegans* and mammalian cells. FERARI plays a key role in Rab11-dependent recycling from sorting endosomes to the plasma membrane. We propose a model in which FERARI supports kiss-and-run of Rab11-positive structures on tubular sorting endosomes to aid the formation of recycling endosomes.

Results

FERARI is a conserved tether

We have recently postulated the existence of a tethering complex containing VIPAS39/SPE-39 and the SM protein VPS-45, which we named FERARI [27]. To probe its existence, we co-expressed *C. elegans* GST-tagged SPE-39 and His-VPS-45 in *E. coli*. His-VPS-45 co-purified with SPE-39-GST (Figure 1a, Extended Data 3d). VPS-33.2, which together with SPE-39 is part of the CHEVI complex [27, 28] served as a positive control, while the HOPS specific VPS-33.1 did not bind SPE-39. These data indicate direct binding of SPE-39 to VPS-45. This interaction was confirmed by yeast-two-hybrid (Y2H) and pull-down experiments (Figure 1b, Extended Data 2d, d', Supplementary Table 3). Moreover, FERARI is conserved in mammalian cells (Figure 1c). VPS45 has been shown to directly interact with rabenosyn-5[29, 30]. Similar to VPS45, rabenosyn-5 interacted with VIPAS39 (Figure 1b-e, Fig. Extended Data 1b, 1b', 2b, 2b', 2d, 2d').

Based on HOPS and CORVET, we speculated that FERARI might contain more subunits (Extended Data 1a). To identify additional components, we incubated the bacterially expressed SPE-39/VPS-45 complex with worm lysate and performed mass spectrometry (Supplementary Table 1), followed by Y2H assays and pull-downs from selected, streamlined candidates. We discovered two additional components of FERARI: the Epsin-homology domain (EHD) containing protein RME-1 and UNC-44 (Figure 1f, Supplementary Table 3).

UNC-44 contains ankyrin motifs and a death domain. SPE-39 interacted well with RME-1 and the ankyrin motifs of UNC-44 (Figure 1f, Supplementary Table 3, Extended Data 1c, 1c',1d, 1d', 2a, 2a'). RME-1 is homologous to mammalian EHD1-4, and UNC-44 to ANK1-3. Since EHD1 has been shown to act at endosomes and EHD2 at the plasma membrane [31, 32], we focused on EHD1. EHD1 co-precipitated and co-localized with rabenosyn-5 (Figure 1h, Extended Data 4a, b). Much less is known about ANK1-3. However, ANK3 appears to be the ANK protein most highly expressed in HeLa cells (Extended Data 4d). ANK3 co-precipitated with endogenous VIPAS39 (Figure 1g). Finally, endogenous VIPAS39 was pulled-down with all other FERARI members (Figure 1d, g, 3f). FERARI members have also other cellular functions, and the deletion of one component did not affect the stability of any other (Extended Data 5a, b). Our experiments revealed the existence of a conserved FERARI tether with a proposed interaction network (Figure. 1i), based on our own data (see also below) and on literature [17, 18, 21, 29, 30]. For clarity, we will use the mammalian nomenclature in the text when referring to FERARI subunits (Figure 1j).

Loss of FERARI affects endosomal recycling

VPS45, rabenosyn-5 and EHD1 have been implicated in recycling from sorting endosomes in mammalian cells [30, 32]. To test whether FERARI might be involved in recycling, we knocked out VIPAS39, VPS45, rabenosyn-5 and ANK3 in HeLa cells expressing GFP-Rab11 (Figure 2a, Extended Data 4c). In FERARI KO cells, Rab11-positive structures were enlarged when compared to control cells (Figure 2a, b). These phenotypes were confirmed by immuno-electron microscopy (Extended Data 6).

To further test whether FERARI plays a role in Rab11-dependent recycling to the plasma membrane, we determined the recycling capacity of transferrin (Tfn). Tfn was transport less efficiently to the plasma membrane in FERARI KO cells (Figure 2c, d). We would not expect a full block because Tfn recycling also occurs through the Rab4-dependent pathway.

The *C. elegans* intestine is an epithelium in which a pair of juxtaposed cells form a tube, the apical gut lumen (Figure 2e). This system provides an excellent system to study membrane traffic in metazoa [12, 33–36]. We used *C. elegans* animals expressing GFP-RAB-11 and RFP-RAB-10, markers for apical and baso-lateral recycling compartments, respectively [37, 38]. In mock treated animals, RAB-11 was mostly localized at the apical cortex, while RAB-10 was present on more internal structures (Figure 2e). Similar to mammalian cells, loss of FERARI caused the enlargement of RAB-11 structures (Figure 2e, Extended Data 5c), indicating that FERARI function is conserved. Even though CHEVI and FERARI share VIPAS39, they have distinct functions because knockdown of VPS33B did not affect RAB-11 localization (Extended Data 7a). Not only apical recycling was perturbed as the tubular part of the RAB-10 compartment was largely extended, while the size of the granular RAB-10 structures remained unchanged (Figure 2e, Extended Data 5c). Human transferrin receptor (hTfR) has been used to study recycling in the *C. elegans* intestine [38]. Knockdown of FERARI led to a strong reduction of the hTfR signal in the gut, suggesting that it less efficiently sorted into recycling endosomes and degraded in the lysosome (Extended Data 7b). In contrast, *VPS33B(RNAi)* caused hTfR to be trapped in a network-like internal structure (Extended Data 7b). We conclude that FERARI plays a role in both apical and baso-lateral recycling. Moreover, CHEVI and FERARI perform distinct functions.

In *C. elegans* oocytes, yolk is taken up by maturing oocytes via receptor-mediated endocytosis employing the yolk receptor RME-2. *FERARI(RNAi)* reduced the level of yolk in oocytes (Extended Data 7c) because of impaired RME-2 recycling (Extended Data 7d). Thus, our data indicate that FERARI is involved in recycling to the plasma membrane in mammalian cells and in different *C. elegans* tissues.

Rab11FIP5 is part of FERARI and provides the link to Rab11

We observed a strong defect upon loss of FERARI function on Rab11 recycling compartments. None of the FERARI components has been shown to directly bind Rab11. However, EHD1 was shown to bind the Rab11 effectors Rab11FIP2 and Rab11FIP5 in mammalian cells [18]. Rab11FIP5, but not Rab11FIP2, co-precipitated with GFP-rabenosyn-5 (Figure 3a, Extended Data 3b, 3b', 3e), indicating that Rab11FIP5 is the link between Rab11 and FERARI. We also confirmed that Rab11FIP5 indeed bound to Rab11 (Figure

3b, Extended Data 3f). To corroborate our findings, we co-expressed VIPAS39 and RAB11 with or without Rab11FIP5 (Figure 3c). While VIPAS39 was barely detected in a RAB11-GFP pulldown, this interaction was substantially stronger in the presence of Rab11FIP5, suggesting that Rab11FIP5 could bridge the interaction between VIPAS39 and RAB11. Moreover, in Rab11FIP5 KO cells, Rab11-positive structures were enlarged and Tfn recycling was impaired similarly to what we had observed for other FERARI members (Figure 3d, e; compare to Figure 2a, Extended Data 7e). Furthermore, the interaction between EHD1 and rabenosyn-5 was weakened in Rab11FIP5 KO cells, and to a lesser extent the interaction between rabenosyn-5 and VIPAS39, suggesting that Rab11FIP5 contributes to FERARI assembly (Extended Data 3c, 3c', Figure 3f). Consistently, Rab11FIP5 co-localized with rabenosyn-5 (Extended Data 4a, b). In *C. elegans*, there is only one homolog of Rab11FIP2 and Rab11FIP5, Y39F10B.1, which we named RFIP-2. *rfip-2(RNAi)* phenocopied the effect of the FERARI(*RNAi*) in the *C. elegans* intestine (Figure 3g, h). Moreover, RFIP-2 physically interacted with FERARI components (Figure 3i, Extended Data 3g). Therefore, we propose that Rab11FIP5 represents one branch of the RAB interaction module of FERARI (Figure 1i, j).

FERARI may act on sorting endosomes

Our data so far suggest that FERARI functions on sorting endosomes. If this interpretation is correct, we might be able to detect an effect on the localization of the Rab proteins on sorting endosomes, RAB-5 and RAB-7. Upon FERARI*(RNAi)*, the RAB-5 signal was more concentrated at the apical membrane and also part of the RAB-7 signal became enriched in the same area compared to mock-treated animals (Figure 4a, b). This finding suggests that reducing recycling capacity could prematurely activate Rab conversion from RAB-5 to RAB-7-positive membranes. If this assumption was correct, disruption of Rab conversion should restore the RAB-5 localization. SAND-1 is part of a RAB-7 GEF complex and a key regulator of Rab conversion [39–41]. Concomitant loss of SAND-1 and FERARI restored RAB-5 localization (Figure 4c, d). Surprisingly, RAB-7 positive compartments were also partially restored under these conditions, even also moderately rescuing the hTfR transport defect (Figure 4c-e). Likewise, the *sand-1 -/-* transport block in coelomocytes was also partially rescued (Extended Data 8a). Thus, loss of FERARI impacts RAB-5 and RAB-7-positive endosomes, consistent with a function of FERARI on sorting endosomes.

FERARI is required SNX-1 active recycling compartment maintenance

The sorting nexins SNX1 and SNX4 in mammals and the *C. elegans* homolog SNX-1 are present on the tubular part of sorting endosomes [42, 43]. Mild overexpression of mCherry-SNX-1 slightly increases the size of tubular portions of sorting endosomes (Figure 5a). To test if the SNX-1 positive tubules are active recycling compartments, we blocked apical recycling by *rab-11(RNAi)*. As expected, the SNX-1 tubules were extended to long networks upon *rab-11(RNAi)*. This finding suggests that RAB-11 drives recycling through these tubules and that the SNX-1 tubules are dynamic structures that respond to recycling flux. Moreover, RAB-5, RAB-7 and RAB-11 co-localized with SNX-1 tubules to a varying degree (Figure 5b, c, movies S1-S4), consistent with the notion that SNX-1-positive structures represent active recycling compartments on sorting endosomes. Of note, the RAB-11 signal was more vesicular and tubular with a rather small contact site. The

Golgi marker MANS-1 and the lipid droplet marker DHS-3 did not show any appreciable co-localization with SNX-1 tubules (Figure 5b, c, movies S6 and S7).

Our data indicate that FERARI and SNX-1 should both be on sorting endosomes. Indeed, EHD1 decorated SNX-1 tubules with discrete puncta (Figure 5b, c, movie S5). When we depleted VIPAS39 or other FERARI components, the association of EHD1 with internal structures was lost, while the plasma membrane pool appeared somewhat less disturbed (Figure 5d). This effect was not due to EHD1 degradation in the absence of FERARI (Extended Data 8b). Thus, EHD1 depends on other FERARI components for recruitment to SNX-1 positive sorting endosomes.

Next, we explored the relationship between SNX-1 and FERARI further. SNX-1 interacted specifically with *C. elegans* VIPAS39 and rabenosyn-5 in Y2H (Figure 5g, Extended Data 1b, 2c, 2c', 3a) and with endogenous VIPAS39 in mammalian cells (Extended Data 8d). Likewise, knockdown of SNX-1 or its interacting partner RME-8 [43, 44] resulted in enlarged RAB-11 positive compartments, indistinguishable from those formed upon loss of FERARI (Figure 5e, f compare to Figure 2e). These data suggest that FERARI and SNX-1/RME-8 act in the same pathway (Figure 1i). More importantly, FERARI*(RNAi)* led to loss of the tubular SNX-1 structures (Figure 5h), indicating that FERARI is involved in the maintenance of SNX-1 recycling compartments. This action appears to be independent of the any potential role of SNX-1 in the retromer pathway, as VPS35, which is part of the cargo selective complex, did not interact with FERARI (Extended Data 8c).

The SNAREs SYX-6 and SYX-7 act in the FERARI-dependent pathway

As a tether FERARI should also contain a functional SNARE binding module. The SM protein VPS-45 was shown to interact directly with SNAREs SYX-7 and SYX-16 [29]. While *syx-7(RNAi)* caused the enlarged RAB-11 compartment phenotype characteristic of FERARI loss, *syx-16(RNAi)* had only a mild effect (Figure 6a, b). In addition, we identified SYX-6 as another potential FERARI SNARE, while VAMP-7 and VTI-1 appeared to have no direct function in RAB-11-dependent recycling. Taken together, our results indicate that FERARI has all the hallmarks of a multisubunit tether in that it possesses a SNARE- and a Rab-interacting module, which could bring two membrane entities together to drive membrane fusion.

Recycling endosome kiss-and-run at sorting endosomes is dependent on FERARI

FERARI is special with respect to the different functions it combines. Next to the classical tethering activities, it also contains EHD1, which acts as a pinchase[14]. Thus, FERARI may promote membrane fission and fusion at the recycling compartment of sorting endosomes. If this was the case, we should detect the arrival of a RAB-11-positive structure at the recycling compartment of the sorting endosome. RAB-11-positive structures docked onto the SNX-1-positive sorting endosome (Figure 6c, movies S8-S10). These RAB-11-positive structures were small with low fluorescence intensities (Figure 6e). We also observed instances in which RAB-11-positive structures were initially docked and then released (Figure 6d, movies S11-S13). Importantly, those RAB-11 endosomes appeared to bigger and brighter (Figure 6e). Using more sophisticated imaging enabled us to visualize RAB-11

dynamics. When we determined the residence time of RAB-11-positive structures on sorting endosomes, we noticed that the individual residence times came in discrete intervals of about 7 sec (Figure 7a, c, Extended Data 9b, movies S14, S15), indicating that the residence time increased in quanta. This quantal behavior was abolished when FERARI function was lost (Figure 7a, c, Extended Data 9b, movie S16). Thus, FERARI is important for RAB-11 recycling endosome fusion and fission at sorting endosomes. A prediction from this model is that cargo molecules should behave in a similar way. hTfR and GLUT1 showed the same FERARI-dependent quantal behavior (Figure 7b, d, e, Extended Data 9c, Extended Data 10, movies S17-S21). We surmise that RAB-11 endosomes picked up cargo and lipids at the sorting endosome, consistent with a kiss-and-run mechanism.

Discussion

How sorting into recycling endosomes occurs at sorting endosomes still remains enigmatic. Here, we report the existence of a multisubunit tether, FERARI, which plays a role in recycling to the apical and basal lateral domains of polarized cells in *C. elegans* and Rab11-dependent recycling in mammalian cells (Extended Data 9a). FERARI represents a tether combining a SNARE-interaction module -VPS45- with Rab interaction modules -Rab11FIP5 and rabenosyn-5[27]. Unlike its relatives, HOPS and CORVET, FERARI tethers membranes containing different Rab proteins. Another remarkable difference is that FERARI contains a dynamin-like protein EHD. This composition provides FERARI with two rather distinct and opposing activities: membrane fission and membrane fusion.

Based on our data, we propose the following model (Figure 7f, movie S22). We assume that FERARI members are recruited onto the sorting endosome by RAB5, where they associate with SNX1 and help to stabilize SNX1-positive structures. At this point we can only speculate about the mechanism. However, ANK3 is known to link membranes to the cytoskeleton and would therefore be well suited to stabilize tubular networks. VPS-45 mediates association with the SNAREs SYX-6 and SYX-7, while RAB11FIP5 will engage with RAB11 on a recycling structure to bring it closer to the sorting endosome. FERARI then would induce SNARE complex assembly and promote membrane fusion, similarly to what has been reported for DSL, HOPS and CORVET [24, 45, 46]. Even though we anticipate full membrane fusion, our data indicate that RAB11-positive membranes do not flatten and retain their globular shape. The barrier for membrane flattening could be provided by EHD1. EHD proteins have been shown to assemble in ring structures similar to dynamin [15, 47]. In this state, cargo to be recycled to the plasma membrane and lipids could diffuse into the RAB11-positive structure. How cargo is enriched in the RAB11 domain, remains unclear. We surmise that back diffusion could be limited by membrane curvature, lipid composition or other proteins. Finally, EHD would promote scission between the RAB11-positive recycling endosome and the tubular part of the sorting endosomes. Our model corresponds to a kiss-and-run model, similar to the one in neurotransmitter release, except that in our case the docked entity is not releasing but rather is taking up content. The ‘flickering’ in the kiss-and-run model of membrane fusion and fission is present in our system and takes about 7 sec (movie S22). In neuroendocrine cells, secretory granules maintain their shape and do not flatten out during fusion with the plasma membrane. Instead, they are released again from the plasma membrane in a process referred to as cavicapture or fuse-

pinch-linger [48, 49]. The coordination of fusion and fission events could be mediated by EHD through interaction with either VPS45 or another SNARE regulator protein, SNAP29 [50]. Thus, FERARI provides a platform on sorting endosomes on which fission and fusion of RAB11-positive structures are coordinated. Rabenosyn-5 could potentially act as the scaffold because it can interact with all FERARI members and sorting nexins.

Our model is supported by our finding that the RAB-11 compartments that dock onto the sorting endosome are smaller than the ones that leave. Moreover, most components of the FERARI have been implicated in recycling previously [17, 21, 26, 28, 51]. Now our data put them into context, providing a temporally and spatially controlled concerted action. FERARI members show a varying degree of co-localization, which might be an indication for dynamic assembly on sorting endosomes. Yet, FERARI was not only involved in RAB11-dependent recycling but also early on in the formation/maintenance of the tubular structures. Rabenosyn-5 and the ANK proteins might be involved in such domain formation. If this hypothesis is correct, we can expect an increase in number of tethering modules on sorting endosomes. In fact, there is already one candidate for such an additional tether. CHEVI has been proposed to act in recycling as well as in α-granule formation, a process which requires TGN to MVB transport [27, 28, 52]. So far only two CHEVI components, VPS33B and VIPAS39, have been identified. Given the localization of these proteins, it is likely that CHEVI acts on sorting endosomes. We propose that tethers could play a role in the formation of domains required for docking on sorting endosomes and likely also on other organelles.

Material and Methods

Worm husbandry

C. elegans was grown and crossed according to standard methods [53]. RNAi was performed as previously described [54]. All experiments were carried out at 20°C, and worms were imaged at the young adult stage (with only few eggs). Worm strains and transgenes used in this study: *bIs1[YP170::GFP + rol-6(su1006)]X, pwIs116 [rme-2p::rme-2::GFP::rme-2 3'UTR + unc-119(+)], pwIs429[vha-6::mCherry-rab-7], pwIs72[vha6p::GFP::rab-5 + unc-119(+)], pwIs90[Pvha-6::hTfR-GFP; Cbr-unc-119(+)], pwIs50[lmp-1::GFP + Cb-unc-119(+)], pwIs414[Pvha-6::RFP::rab-10, Cbr-unc-119(+)], pwIs69[vha6p::GFP::rab-11 + unc-119(+)], pwIs782[Pvha-6::mCherry::SNX-1], pwIs87[Pvha-6::GFP::rme-1; Cbr-unc-119(+)], [Pdhs-3::dhs-3::GFP], pwIs481[Pvha-6::mans-GFP, Cbr-unc-119(+)].*

Microscopy

Living worms were imaged as described [54]. Levamisole (50 mM) was used for immobilization, and 2% agarose pads were cast onto microscopy slides; worms were sealed under cover slips using vaseline. Images were acquired using a spinning disk confocal system Andor Revolution (Andor Technologies, Belfast, Northern Ireland) mounted onto an IX-81 inverted microscope (Olympus, Center Valley, PA), equipped with iXon^{EM}+ EMCCD camera (Andor Technologies). A 63x 1.42 N.A. oil objective was used, where each pixel represents 0.107 μm. Solid-state 488 nm and 560 nm lasers were used for excitation and exposure time was 100 ms. Images were averaged 4 times for oocytes and 32 times for

intestine and coelomocytes. Alternatively, an Olympus Fluoview FV3000 system with a high sensitivity-spectral detector (HSD) was used (PTM voltage= 500). The objective was 60x with silicone oil, and the Galvano scan device was used. Pixel size corresponds to 0.098 μm. Sampling speed was 8.0 μs/pixel, zoom= 2.1, lasers 488 (GFP) or 561 (RFP, mCherry) were set at 4-10%. All images were processed in the same way for corresponding experiments.

Images of SNX-1 tubules with different GFP markers were obtained on a Zeiss LSM 880 microscope with Airyscan. The fast mode was used and images were processed using the Zen Black software. Worms were treated with 20 mM sodium azide to avoid any movement during image acquisition.

Movies with SNX-1 and RAB-11, hTfR or Glut1 markers were taken on the LSM 880 Airyscan microscope, using the fast mode. Reducing the averaging to 2-4 times resulted in frame speeds of 0.5 -1.0 seconds that were appropriate to the speed of the vesicles. Movies covered about 2 intestinal cells (about 70 μM square). Worms were treated with 50 mM Levamisole and imaged as fast as possible to avoid loss of endosomal movement in the gut cells. Worms in the correct stage showed reticulated SNX-1 compartments with extruding and contracting tubules that coincided with active vesicle movement. Several movies were taken per worm and resulted in up to 5 vesicles showing “kiss & run” behavior per movie. Small movies covering only one vesicle movement were collected from the larger movies and used to quantify the residence times. The “StackReg” plugin was very useful to remove the shifting worm motions and allow good tracking of single vesicles from frame to frame.

Immuno EM

HeLa cells transfected with Rab11-GFP were prepared for immuno-labelling as described in [55]. The first antibody was rabbit anti-GFP (1:100; Abcam 6556) and the secondary was goat anti-rabbit coupled to 10 nm gold particles (BB International).

Interaction studies with worm proteins

C. elegans proteins SPE-39 and VPS-45 were expressed in *E. coli* Rosetta (DE3) cells. GST-tagged SPE-39 was obtained by cloning the worm cDNA into pETGEXCT vector, while His-tagged VPS-45 cDNA was cloned into pRSF-2 Ek/LIC vector. 500 ml *E. coli* cultures bearing both plasmids (grown in LB+amp+kan) were induced with 0.5 mM IPTG overnight at 37°C and collected in buffer with 50 mM HEPES pH 7.7, 300 mM NaCl, 10% glycerol and 1% TritonX 100 (with protease inhibitors) for purification. Cells were lysed with 1 mg/ml lysozyme, 20 μg/ml DNaseI and 2x 30 sec sonication. After a 16,000 g spin, the cleared lysate was incubated overnight with Ni-NTA beads. Beads were washed 4x and eluted with 250 mM Imidazole. The eluate was pooled and bound overnight to glutathione beads. Worm lysate from 100 ml liquid culture (with many adults) was prepared in the same buffer (with glass beads in a FastPrep machine for 2x 30 sec). The worm extract was centrifuged at 16,000 g for 30 min to yield a clear worm lysate that was added to the washed Glutathione beads with bound SPE-39/VPS-45 complex. Proteins were allowed to bind overnight and finally the beads were washed 4x with lysis buffer and 4x with lysis buffer lacking any kind of detergents for mass spectroscopy analysis. Proteins were kept at 4°C at all times.

Quantification of bands both in mammals and *C. elegans* was performed on non-overexposed bands for 3 western blots each (N=3). Band-sized regions of interest of the same size were used to determine the mean grey values of bands in ImageJ. Inputs and pull-downs were measured and adjusted for the amounts of protein loaded. Percentage of pull-down was calculated for bait protein and prey protein. The percentage of interaction was normalized to the bait (assuming that full interaction could only be achieved if all the bait was pulled down, e.g. if 30% of the bait and 15% of the prey were pulled-down, this would correspond to 50% interaction between prey and bait).

Yeast two hybrid assays were carried out using worm cDNA cloned into the vectors pEG202 (with DNA binding domain DBD) and pJG4-5 (with activation domain AD). Fastest results were obtained by Gibson Assembly cloning (NEBuilder, NEB; E55205). pEG202 clones also obtained a 3xFLAG tag at the C-terminus for pull-down experiments. Growth assays were carried out with 6 colonies from yeast transformation (strain EGY48+pSH18-34 plasmid for LacZ expression) for 3-7 days at 30°C on plates lacking leucine and with addition of 2% galactose for induction of pJG4-5 expression. For pull-down experiments, 50 ml cultures of yeast were induced with 2% galactose at OD_{600}= 1.0 for 6 hours. Cells were lysed in 50 mM HEPES pH 7.7, 300 mM NaCl, 10% glycerol and 1% TritonX 100 (with protease inhibitors) in a FastPrep device (2x 30 sec). 25 µl of magnetic beads (slurry) were added for binding of tagged proteins (either anti-HA (Pierce; 88837) or anti-FLAG beads (Sigma; M8823)) and rotated overnight. After 4x washing, proteins were eluted with Laemmli sample buffer at 95°C for 5 min and applied to SDS-PAGE gels for immunoblot analysis with FLAG and HA antibodies (FLAG: Sigma; F3165, HA: Sigma HA-7 clone; H9658).

Cell culture, transfection and CRISPR/CAS9 knockout in mammalian cells

HEK293 and HELA cells were cultured and maintained in DMEM (Sigma) high glucose medium with 10% FCS (Bioconcept), penicillin–streptomycin (1%), sodium pyruvate and L-glutamine. Cells were plated 1 d before transfection at 60-70% confluency and later transfected for 48 h using Turbofect transfection reagent (Thermo Scientific; R0532) according to the manufacturer's instructions. 2-5 µg of DNA was used per reaction based on a 10 cm dish.

For CRISPR/Cas9-mediated knockout, guide RNAs were selected using the CRISPR design tool (http://chopchop.cbu.uib.no/). A list of oligos is given in Table S2. Two guide RNAs were designed from two different exons for each target gene. Annealed oligonucleotides were cloned into two different plasmids, Px458 GFP and Px459 Puro, respectively. In brief, HELA cells were seeded at 2×10^6 cells per 10 cm dish. The following day, cells were transfected with 2.5 µg of the plasmids (control vectors without insert or vectors containing a guide RNA against target gene). Transfecting media was exchanged with fresh media after 4 h. Cells were treated with puromycin for 24 h after transfection followed by FACS sorting (for GFP+ cells) on next day. For FACS sorting after 48 h of transfection, cells were trypsinized and resuspended in cell-sorting medium (2% FCS and 2.5 mM EDTA in PBS) and sorted on BD FACS AriaIII Cell Sorter. GFP-positive cells were collected and seeded in a new well.

Immunoprecipitation assays

HEK-293 cells were co-transfected with indicated DNA constructs. After 36-48 h of transfection, protein extracts were prepared in lysis buffer (1% NP-40, 50 mM Tris/HCl pH 7.5, 150 mM NaCl) and Halt protease inhibitor cocktail (Thermo Scientific; 186 1279) at 4°C for 20 min followed by centrifugation at 4°C for 20 min at 13,000 rpm. Immunoprecipitations were performed as previously described [56]. In brief, protein extracts were incubated with trap beads (nano bodies for GFP (GFP-Trap®_A; gta-20-chromotek), myc (Myc-Trap®_A; yta-20-chromotek), turbo-GFP (TurboGFP-Trap_A; tbta-20-chromotek)) for 4 h at 4 °C with rotation, and then washed 5x with lysis buffer (1 ml). Protein complexes were eluted by heating beads for 5 min at 95°C in 2x sample buffer and resolved by SDS-PAGE on 10% and 12.5% gels followed by immunoblot analysis. Blots were developed using Amersham ECL Prime Western Blotting Detection Reagent (RPN2236) and X-ray film (Amersham Hyperfilm ECL-28906839).

Western blot analysis

Cells were collected and lysed in lysis buffer (50mM Tris/HCl, 150 mM NaCl, 1% NP-40) containing a protease inhibitor cocktail (Roche). Protein concentrations were determined in all experiments using the Bio-RAD protein assay (Bio-RAD, 500-0006) and 20-40 μg of total protein was loaded onto either 10 or 12.5 % SDS-PAGE before transfer onto nitrocellulose membranes (Amersham Protran; 10600003). Membranes were blocked 5% milk, 0.1% Tween20 for 60 min at RT. First antibody incubation was O/N at 4°C and the secondary HRP coupled antibodies incubated for 1 h at RT. The blots were developed using Amersham ECL Prime Western Blotting Detection Reagent (RPN2236) and X-ray film (Amersham Hyperfilm ECL-28906839) or the Fusion FX7 (Vilber Lourmat) image acquisition system.

Antibodies

The antibodies used in this study: polyclonal rabbit anti-VIPAS39 (20771-1-AP; proteintech; 1:2000), polyclonal rabbit anti-Rab11-FIP5 (NBP1-81855; Novus Biologicals;1:2,000), polyclonal rabbit anti-EHD1 (NBP2-56035; Novus Biologicals; 1:2,000), polyclonal rabbit anti-rabenosyn-5 (NB300-813; Novus Biologicals; 1:2,000), monoclonal mouse anti-myc (9E10) (1:3,000 for WB and 1:200 for Immunostaining; Sigma-Aldrich; M4439), polyclonal rabbit anti-GFP (TP401; Torrey Pines; 1:3,000 for WB and 1:200 for Immunostaining). For pulldowns Trap beads (Nano bodies) were used. GFP-Trap_A (chromotek, gta-20) for GFP pulldowns and myc-Trap_A (chromotek; yta-20) for myc pulldowns. HRP-conjugated goat anti-Mouse IgG (H+L) Secondary Antibody (Thermo Fisher scientific; 31430; 1:10,000), polyclonal HRP conjugated goat-anti-rabbit IgG (Thermo Fisher scientific; 31460; 1:10,000) were used (incubated for 1 h at RT) to detect bound antibodies with and an ECL system (ECL prime, Amersham, RPN2232). Alexa Fluor 488-goat anti-rabbit IgG (H+L) (Invitrogen; A-11034) and Alexa Fluor 594-goat anti-mouse IgG (H+L) Cross-Adsorbed Secondary Antibodies (Invitrogen; R37121) were used for immunofluorescence.

Immunostaining in mammalian cells

Cells were plated onto sterile 13 mm glass coverslips. Cells were fixed with 2% paraformaldehyde for 15 min, permeabilized (0.1% TritonX 100 in PBS) for 5 min and blocked with 2% BSA containing 5% goat serum in PBS for 1 h. Cover slips were incubated in Primary antibodies for 2 h and washed in PBS for 5x followed by 1 h incubation in fluorescently-tagged secondary antibodies. After secondary antibody incubation, cover slips were washed again 5x in PBS and mounted onto glass slides using Fluoromount-G (Southernbiotech; 0100-01). Images were taken with an inverted Olympus FV1000 confocal microscope using a Plan Apochromat N 60x/1.40 silicon oil objective with z-stacks. Co-localization studies were performed using the ImageJ co-localization plugin JACoP.

Transferrin (Tf) recycling assay

Recycling assay was mainly performed according to [57], with some modifications. For immunoblot, 600,000 cells were grown in a 6-well plate. The following day, cells were starved for 1 h in serum-free medium at 37°C and then treated with 20 μg/ml of Transferrin biotin for 1 h in serum free medium. Cells were then chased with holo transferrin (100 ug/ml) and defuroxamine mesylate (100 μM; to prevent re-internalization) in serum containing medium for different time points. At the end of each time point, cells were washed three times with ice-cold PBS and treated with proteinase K (500 g/ml) for 30 min. To neutralize Proteinase K, cells were treated with 2x PMSF for 10 min. Cells were collected in microfuge tube and washed twice with ice cold PBS. Cells were lysed with lysis buffer and subjected to immunoblot with streptavidin HRP.

For imaging, cells were grown in 8-well imaging chambers. The following day, cells were starved for 1 h in serum-free medium at 37°C and then treated with 10 μg/ml of Transferrin-Alexa-594 for 1 h in serum free medium. Cells were then chased with holo transferrin (100 μg/ml) and defuroxamine mesylate (100 μM; to prevent re-internalization) in serum containing medium for different time points. At the end of each time point, cells were washed once with ice cold PBS and treated with 0.1M glycine (pH 3.5) for 45 seconds followed by wash in ice cold PBS for two times, fixed in 4% PFA followed by washing with PBS. Cells were then permeabilized with 0.1% Triton X100 for 5 min, washed three times with PBS. Cells were covered with ibidi mounting medium for imaging.

Live cell imaging

For live imaging, cells were plated in 8-well chambered coverglass and media was replaced with warm imaging buffer (5 mM dextrose (D(+)-glucose, H_2O, 1 mM $CaCl_2$, 2.7 mM KCl, 0.5 mM $MgCl_2$ in PBS) just before imaging. Images were taken at 37°C on an inverted Axio Observer Zeiss microscope (Zeiss, Oberkochen Germany) using a Plan Apochromat N 63×/1.40 oil DIC M27 objective with a Photometrics Prime 95B camera. Z-stack images were processed by using the OMERO client server web tool and Fiji.

DNA plasmid sources

Commercially available Plasmids were obtained from Addgene and Origene. VPS33B-Myc-DDK (Origene; RC203870), Myc-DDK-VIPAS39 (Origene; RC202264), GFP-VIPAS39 (Sino.Bio; HG22032_ACG), Myc-DDK-VPS45 (Origene; RC206027), Turbo-GFP-VPS45

(Origene; RG206027), Myc-DDK-rabenosyn-5 (Origene; RC239555), GFP-rabenosyn-5 (Addgene; 37538), RFP-rabenosyn-5 (Addgene; 37537), GFP-RAB11 (Addgene; 12674), Myc-DDK-ANK1 (Origene-RC220763), Myc-DDK-FIP5 (Origene; RG206173), Myc-DDK-EHD1 (Origene; RC211158), Myc-DDK-FIP2 (Origene; RC210414). Plasmids Px458 GFP (Addgene; 48138) and Px459 Puro (Addgene; 62988) were used for cloning gRNAs.

Compartment quantifications

The length of RAB-10 tubules was measured by applying a freehand line ROI in one z plane, for size of RAB-11 compartments the elliptical selection tool was used and the area in pixels was measured. Both methods might lead to an underestimate of the real sizes, because tubules and globular compartments were not measured in 3D projections, but the differences between wild-type and mutant phenotypes were sufficiently large so that more complicated quantification methods were not essential. In all cases, 6 different worms were analysed and 10 structures per worm were measured (in different z planes).

The size of RAB-10 globular compartments could be measured in a more automated way because they are very bright and sufficiently separated from each other (in contrast to RAB-11 where only the outlines of the enlarged compartments were visible and vesicles clustered together). Maximal z projections were carried out on the whole stack of pictures, yielding about 50-120 vesicles per worm (6 worms per condition were measured). Threshold was set and the pictures were transformed into binary images. The “close-” and “watershed” function was applied to get rid of single pixels and fused objects. Particles were analysed (size setting= 0-infinity and circularity= 0.5-1.0). Extremely large accumulations of objects that escaped the “watershed” function were manually excluded from the final analyses.

Quantification of Rab11-positive endosomes

Segmentation and analysis were performed on manually chosen regions of interest (ROI) using a custom script for Fiji[58] as follows: 1) A 3D White Top-Hat filter [59] was applied to the original image in order to homogenize the background and used to compute 3D seeds[60] with subpixel accuracy. 2) Objects were segmented on the original image using an iterative threshold[61] and converted to labels. 3) Touching objects were then separated by a 3D watershed[62] using the previously identified seeds on the label image. 4). The resulting image was then added to the 3D ROI Manager[10] to exclude remaining laterally touching objects and finally perform intensity and size measurements per object. 1,500-2,500 Rab11-positive particles were analyzed from 45-60 cells for each condition. The script is available upon request.

Quantification of Corrected total cell fluorescence (CTCF) measurement for transferrin recycling assay

Cells were selected by freehand drawing tool in ImageJ. To obtain background reading a region next to the cell that has no fluorescence area was also selected. Integrated density and mean grey values of the selected areas were measured. Following formula was used to measure CTCF. CTCF = Integrated Density – (Area of selected cell X Mean fluorescence of background readings).

Normalized value of three independent experiments was averaged.

Quantification of western blot data

Immunosignals of different proteins (antibodies) were quantified in ImageJ software. The intensity of the loading control immunosignals was used for normalisation to ensure equal protein contents of the lysates. Normalized value of three independent experiments was averaged.

RNA isolation, cDNA preparation and quantitative real-time PCR (qPCR)

Total RNA was collected from human cells by using RNeasy mini kit (QIAGEN_74104) according to the manufacturer's protocol. Afterwards, 1000 ng RNA was reverse transcribed into cDNA using cDNA Synthesis Kit GoScript™ Reverse Transcriptase and GoScript™ buffer mix oligo-dT (Promega_A2791) following the instructions given by the suppliers. 250 nM primers and 3 μl of the cDNA product was then used for quantitative real-time-PCR using GoTaq® qPCR Master Mix (Promega_A600A) supplemented with CXR Reference Dye (Promega_C541A) that was then analyzed using a StepOnePlus™ Real-Time PCR System (Applied Biosystem). The relative levels of the target transcripts were determined using the human beta actin transcript as reference.

Statistics and reproducibility

All immunoblots were performed at least three times unless otherwise noted in the legend. GraphPad Prism 8.0.2, Excel 2016 were used for the statistical analyses. Statistical analysis was performed using two-tailed t-tests.

Extended Data

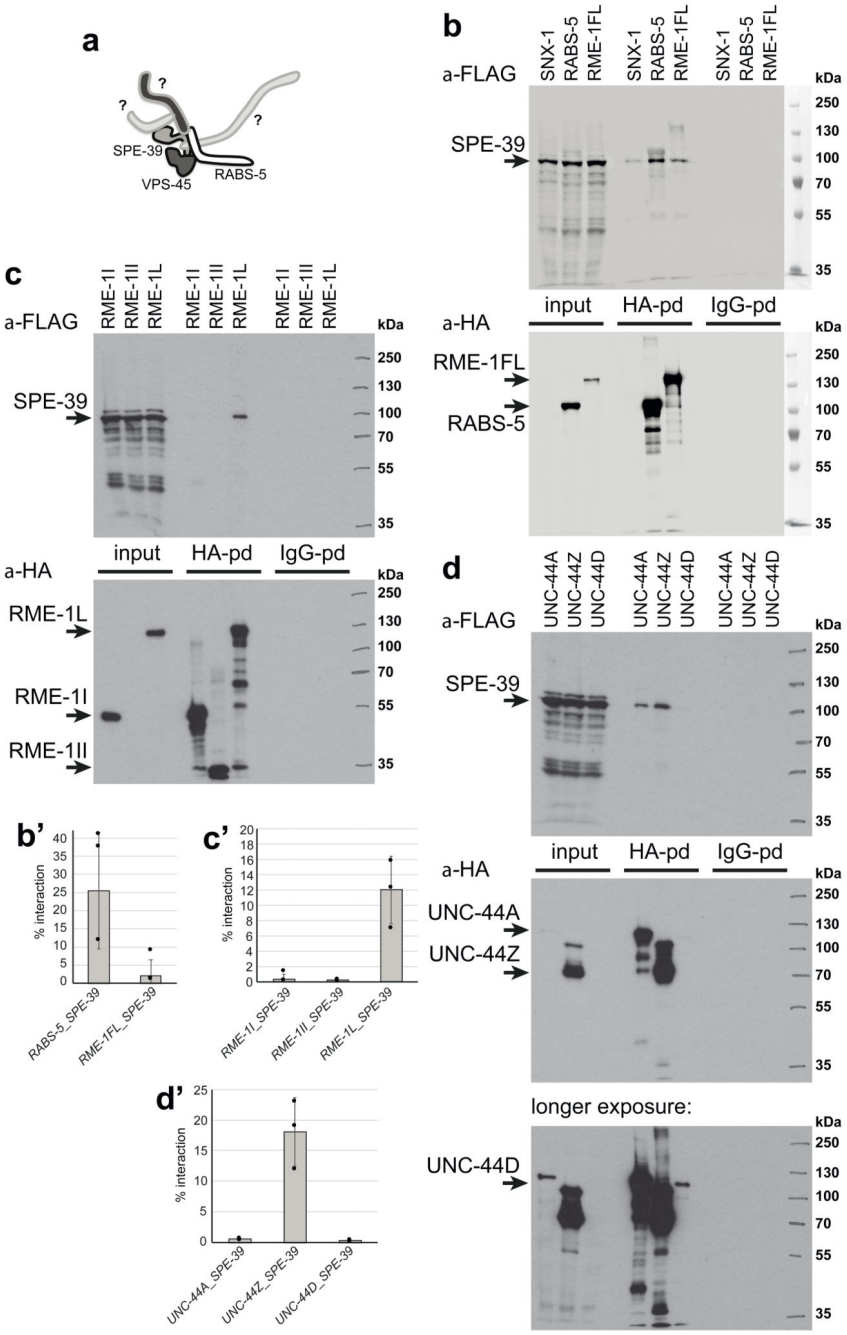

Extended Data Fig. 1. Pull-downs of FERARI subunits show multiple interactions.

(a) Schematic drawing of the putative FERARI tether. (b) Pull-downs were performed with extracts from yeasts expressing SPE-39-FLAG and the HA-tagged proteins indicated at the top. Control pull-downs with beads coupled to IgG were also carried out. Arrows on the left indicate the sizes of expressed proteins. n=3 independent experiments. Quantification is shown in (b'); mean ± s. d. is given. (c) Pull-downs showing interactions between

SPE-39-FLAG and HA-RME-1 fragments. n=3 independent experiments. Quantification is shown in (c'); mean ± s. d. is given. (d) Pull-downs experiments using SPE-39-FLAG and fragments of UNC-44 (with HA tag). UNC-44D fragment expression is low and can be seen on longer exposure as indicated. n=3 independent experiments. Quantification is shown in (d'); mean ± s. d. is given. See Unprocessed Blots Extended Data 1 and Statistical Source Data Extended Data 1.

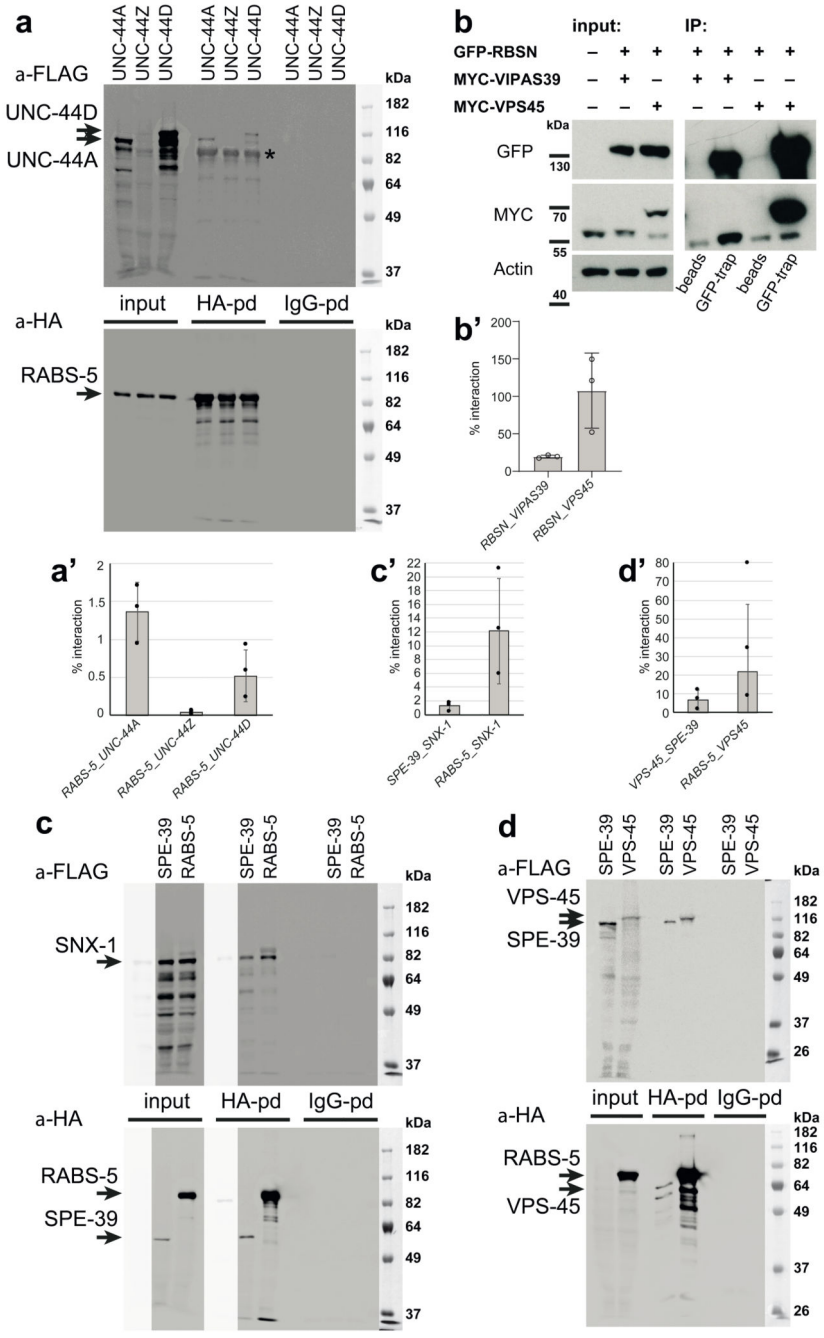

Extended Data Fig. 2. Determination of FERARI subunits interactions.

Europe PMC Funders Author Manuscripts

Europe PMC Funders Author Manuscripts

(a) Pull-downs showing interaction between HA-RABS-5 and fragments of UNC-44 (coupled to FLAG). UNC-44Z was not expressed, anti-FLAG antibody cross-reacted with RABS-5 (indicated by asterisk). n=3 independent experiments. Quantification is shown in (a'); mean ± s. d. is given. (b) Western blot of the interactions between transiently over-expressed human FERARI components rabenosyn-5, VIPAS39 and VPS45. GFP-Rabenosyn-5 was precipitated with GFP-trap beads, and myc-VIPAS39 and myc-VPS45 co-precipitated. n= 3 independent experiments. Quantification is shown in (b'); mean ± s. d. is given. (c) Pull-down experiment showing the interaction of SNX-1 with SPE-39 and RABS-5. n=3 independent experiments. Quantification is shown in (c'); mean ± s. d. is given. (d) Interactions between SPE-39 and VPS-45 as well as VPS-45 and RABS-5 in pull-down experiments. n=3 independent experiments. Quantification is shown in (d'); mean ± s. d. is given. See Unprocessed Blots Extended Data 2 and Statistical Source Data Extended Data 2.

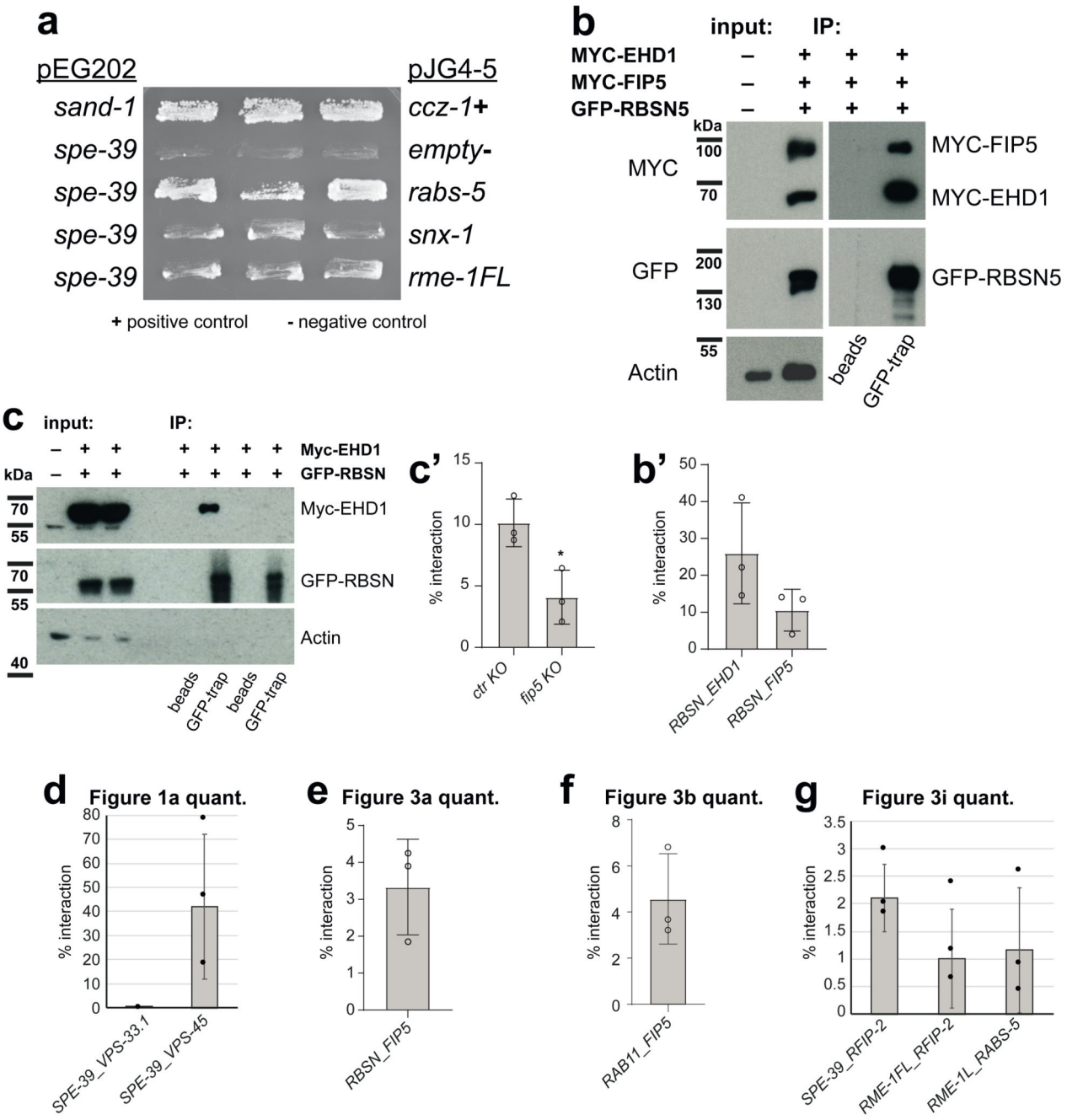

Extended Data Fig. 3. Interactions of *C. elegans* and mammalian FERARI subunits.

(a) Yeast two hybrid growth assay showing interactions between SPE-39 (bait) and RABS-5, SNX-1 and RME-1 (preys). n=3 biologically independent experiments. (b) Western blot depicting the interactions between human protein Rabenosyn-5 with EHD1 and Rab11FIP5, co-expressed in HEK-293 cells. GFP-Rabenosyn-5 was used as bait to co-immunoprecipitate myc-tagged EHD1 and Rab11FIP5. n= 3 independent experiments. Quantification is shown in (b'); mean ± s. d. is given. (c) Interaction between RBSN and EHD1 is reduced in rab11fip5 KO cells. ctr KO and rab11fip5 KO HEK293 cells were

Europe PMC Funders Author Manuscripts

co-transfected with GFP-RBSN and myc-EHD1 as indicated and myc-trap beads were used as bait. Immunoprecipitated proteins and inputs were then probed with antibodies against myc, GFP and actin. n=3 independent experiments Quantification is shown in (c'); mean ± s. d. is given (P=0.0232). (d) Quantification of interactions shown in Fig. 1a, (e) Fig. 3a, (f) Fig. 3b and (g) Fig. 3i. The mean values ± standard deviations are shown; n=3 independent experiments; *P < 0.05, **P < 0.01, ***P < 0.00, ****P < 0.0001, and n.s. P > 0.05. Two-tailed Student's t-tests were used for all analyses. See Unprocessed Blots Extended Data 3 and Statistical Source Data Extended Data 3.

Europe PMC Funders Author Manuscripts

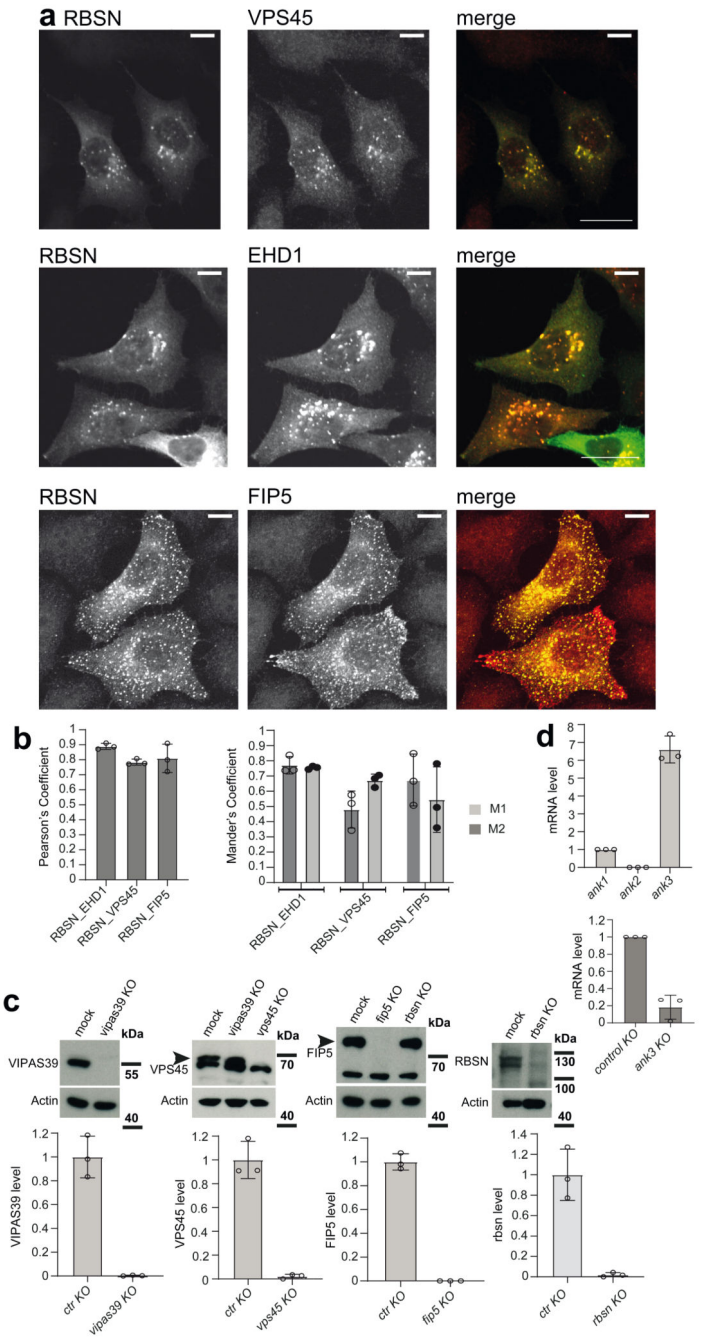

Extended Data Fig. 4. Human FERARI components interact and co-localize in HeLa cells.

(a) Co-localization of rabenosyn-5 with human FERARI components VPS45, EHD1, and Rab11FIP5. HeLa cells co-transfected with GFP-Rabenosyn 5 and myc-VPS45, myc-EHD1, myc-Rab11FIP5 were subjected to immunofluorescence staining with GFP and myc antibodies. (b) Quantification of co-localization shown in (a). n=95 cells were analyzed from n=3 independent biological replicates. Data show the mean ± s.d. (c) Western blot depicting the efficiencies of CRISPR-Cas9 KO of indicated proteins in HeLa cells used for analyses in Fig. 2A and 3C. Corresponding quantifications are shown below each western blot. n=3

independent biological replicates (Data show the mean ± s.d). (d) RT-qPCR data represents levels of ank1, ank2 and ank3 mRNA in HeLa cells at endogenous level and in the ank3 KO. n= 3 independent experiments Data show the mean ± s.d. See Unprocessed Blots Extended Data 4 and Statistical Source Data Extended Data 4.

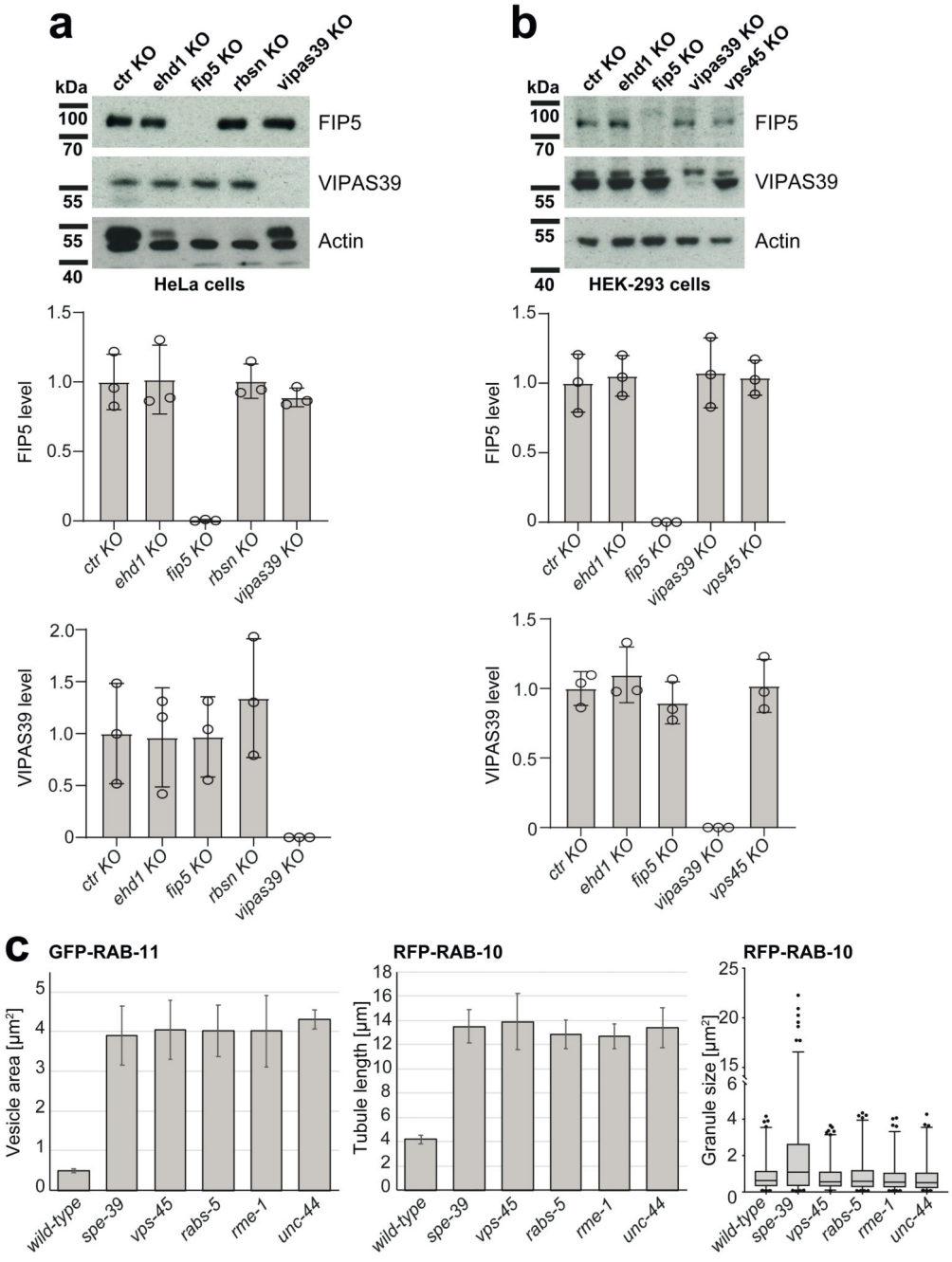

Extended Data Fig. 5. Analysis of FERARI platform stability and phenotype.

(a & b) Protein stability of FERARI components in the KO cells. Endogenous levels of Rab11FIP5 and VIPAS39 were assessed in different FERARI KO HeLa (a) and

Europe PMC Funders Author Manuscripts

HEK-293 (b) cell lines as indicated. n=3 independent biological replicates. Data show the mean ± s.d. (c) Quantification of RAB-11 and RAB-10 phenotypes shown in Fig. 2E. RAB-11 compartments and RAB-10 tubules were measured in n=6 worms (n=10 structures each), RAB-10 globular compartments were quantified semi-automatically and comprise N=50-120 structures (per worm) in n=6 different worms. Mean ± s.d. is given. For the box plot, the box represents 25-75 percentile box with median and the whiskers 1-99 percentile. See Unprocessed Blots Extended Data 5 and Statistical Source Data Extended Data 5.

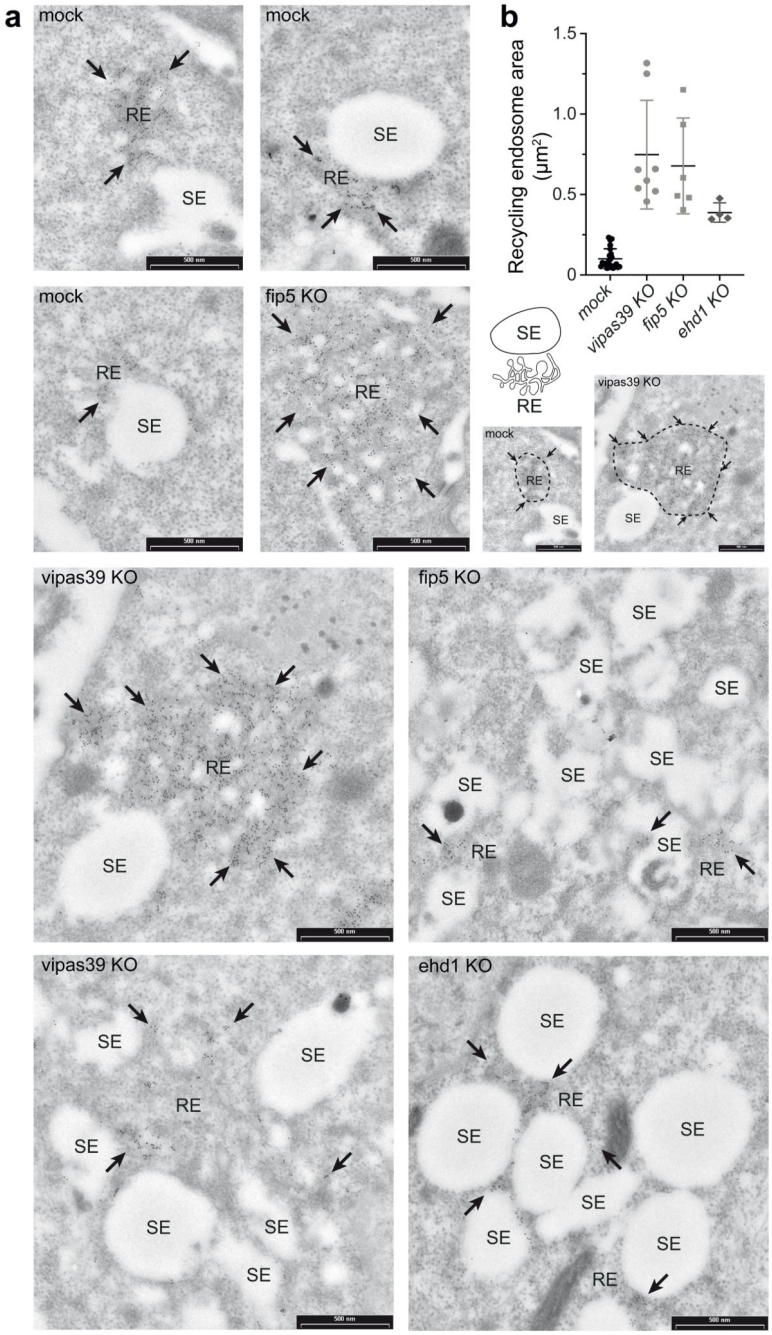

Europe PMC Funders Author Manuscripts

Europe PMC Funders Author Manuscripts

Extended Data Fig. 6. Morphology of Rab11 compartments is affected by FERARI knock-downs in HeLa cells.

(a) Electron micrographs showing the structure of immunogold labeled Rab11 compartments. HeLa cells with the indicated CRISPR knock-outs were processed for immuno-electron microscopy. Globular sorting endosomes are marked with “SE”. Tubular recycling endosomes with Rab11 signals are marked with “RE”. Arrows point to densely labeled Rab11 structures containing tubular membranes. Scale bars: 500 nm. (b) Quantification of recycling endosome sizes in different KO HeLa cells shown in (a). n=23 for mock, n=8 for vipas39 KO, n=6 for rab11fip5 KO and n=4 for ehd1 KO cells (mean ± s.d.). n: number of cells. A schematic representation of sorting endosomes (SE) and recycling endosomes (RE) is shown. For size measurements the recycling endosomes were encircled as shown in the example pictures below the graph. Scale bars: 500 nm. See Statistical Source Data Extended Data 6.

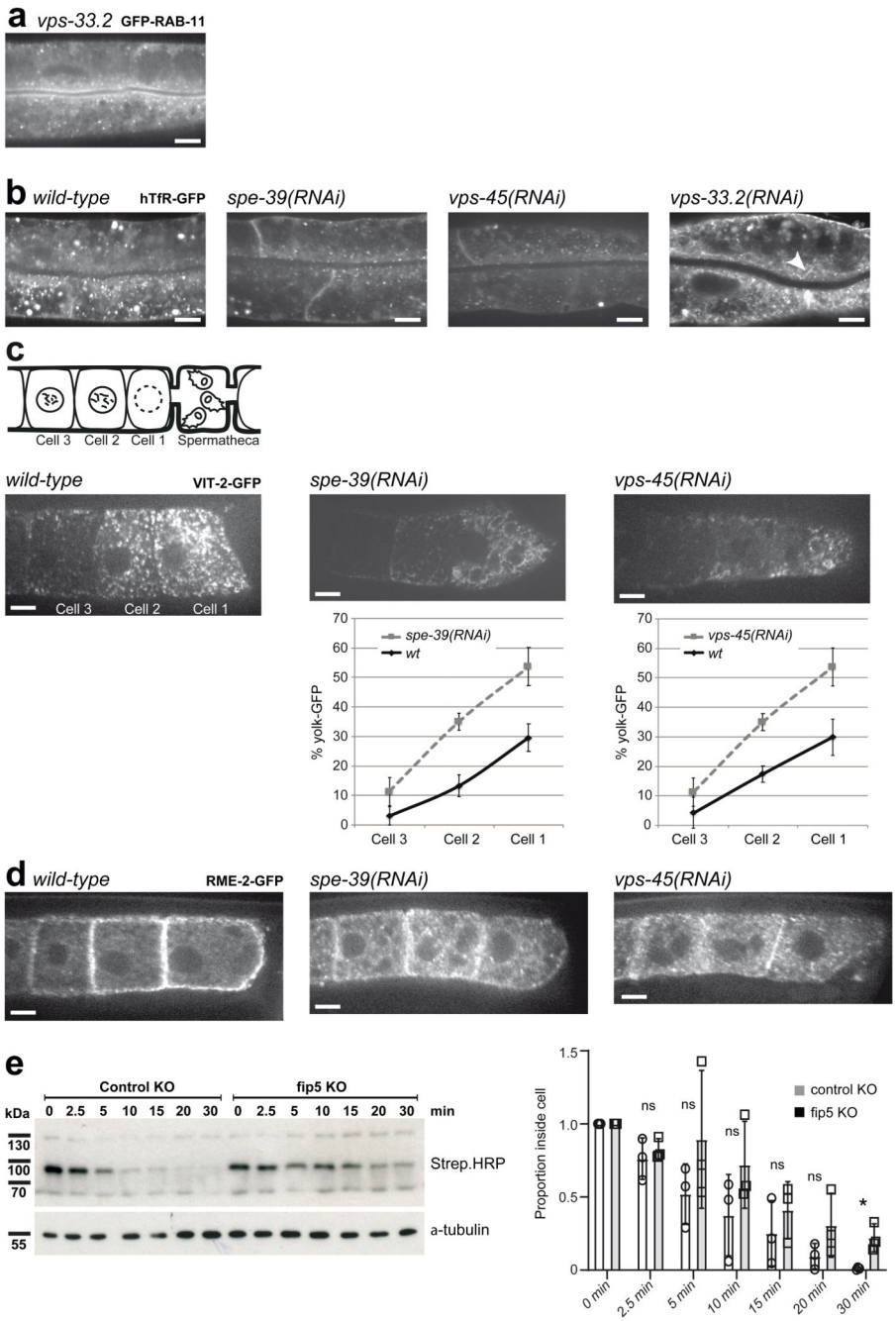

Extended Data Fig. 7. Function of *spe-39* and v*ps-45* in endosomal recycling.

(a) Knock-down of *vps-33.2* in worms has no effect on RAB-11 compartments. n=3 independent RNAi experiments with n=20 animals. Scale bar: 10 µm. (b) Recycling of hTfR-GFP is abolished in *spe-39(RNAi)* and *vps-45(RNAi)* worms but not in *vps-33.2(RNAi)*. Most hTfR-GFP signal is lost in *spe-39(RNAi)* and *vps-45(RNAi)* worms. n=3 independent RNAi experiments with n=20 animals. Scale bars: 10 µm. (c) Schematic representation of the last 3 oocytes prior to the spermatheca in the worm gonad. Yolk uptake defect of *spe-39(RNAi)* and *vps-45(RNAi)* worms. n=3 independent RNAi experiments with

n=20 animals. Wild-type uptake of VIT-2-GFP was quantified in the first 3 oocytes before the spermatheca. The measurements were normalized to the total fluorescent signal of all 3 wild-type cells. Knock-down of *spe-39* and *vps-45* show a reduction of yolk uptake. n=6 gonads were quantified for each RNAi experiment. Scale bars: 10 μm. (d) The yolk receptor RME-2-GFP is mis-localized in *spe-39(RNAi)* and *vps-45(RNAi)* worms. n=3 independent RNAi experiments (n=20 animals). Scale bars: 10 μm. (e) Transferrin recycling in HeLa cells is reduced in rab11fip5KO Hela cells. After 1 h starvation ctrl KO and rab11fip5KO cells were treated with Transferrin Biotin. Cells were then chased with holo transferrin up to 30 min, and cell lysates were subjected to immunoblot with Streptavidin HRP. Quantification of the immunoblot: The mean ± s.d. values are shown; n=3 independent experiments. (P= 0.5249 at 2.5 min; P=0.2764 at 5 min; P=0.2169 at 10 min; P=0.4093 at 15 min; P=0.1949 at 20 min; P=0.01901 at 30 min). *P < 0.05, **P < 0.01, ***P < 0.00, ****P < 0.0001 and n.s., P > 0.05. Two-tailed Student's t-tests were used for all analyses. See Unprocessed Blots Extended Data 7 and Statistical Source Data Extended Data 7.

Europe PMC Funders Author Manuscripts

Europe PMC Funders Author Manuscripts

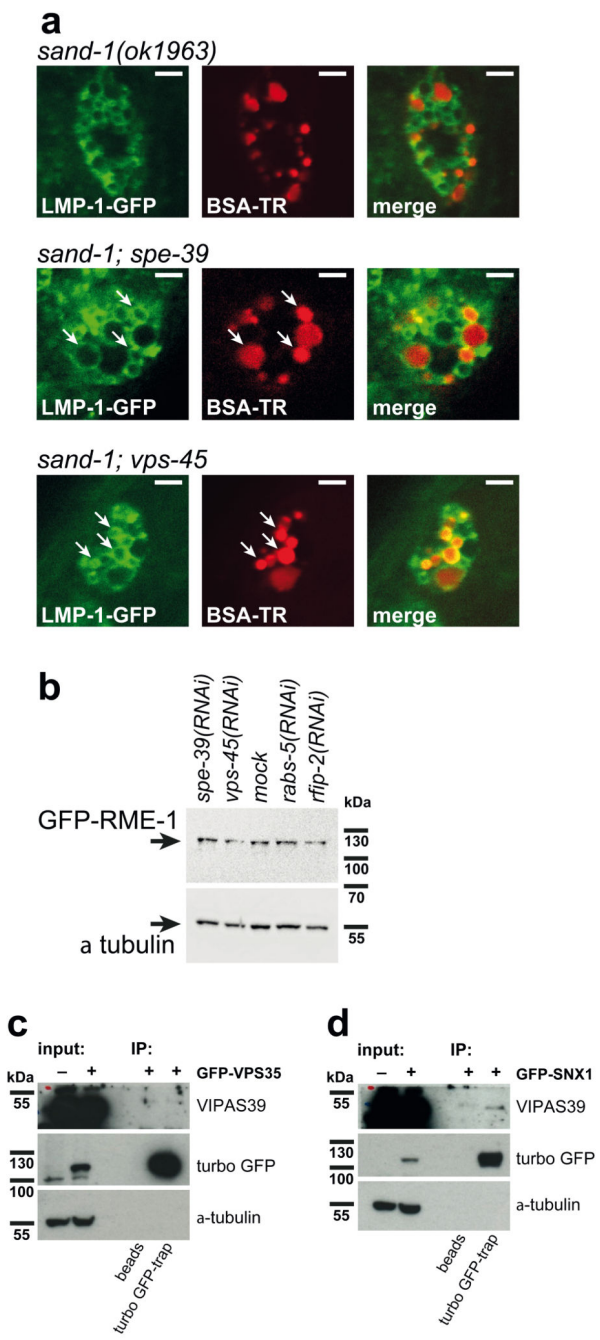

Extended Data Fig. 8. Loss of recycling by *spe-39(RNAi)* or *vps-45(RNAi)* partially rescues a sand-1 mutant and endogenous VIPAS39 interacts with SNX1.

(a) Knock-down of spe-39 or vps-45 induces the degradation pathway in coelomocytes. In *sand-1(ok1963)* coelomocytes BSA-TR is not transported to the lysosomes (LMP-1 compartment). *spe-39(RNAi)* and *vps-45(RNAi)* will favor the transport of BSA-TR to coelomocytes, probably by abolishing recycling. Arrows indicate LMP-1-positive compartments containing BSA-TR. n=3 independent RNAi experiments (n=20 animals). Scale bars:5 μm. (b) GFP-RME-1 levels were unchanged upon *FERARI (RNAi)*. Western blot analysis of GFP-RME-1 levels in *FERARI(RNAi)* worm lysates. n=3 independent

experiments. (c) Endogenous VIPAS39 does not interact with Retromer subunit VPS35 in HEK-293 cells transfected with GFP-VPS35. n=3 independent experiments. (d) GFP-SNX1 transfected HEK-293 cells show slight interaction between SNX1 and endogenous VIPAS39. n=3 independent experiments. Very weak interaction (< 1%) could not be measured due to overexposed bands in the input. See Unprocessed Blots Extended Data 8.

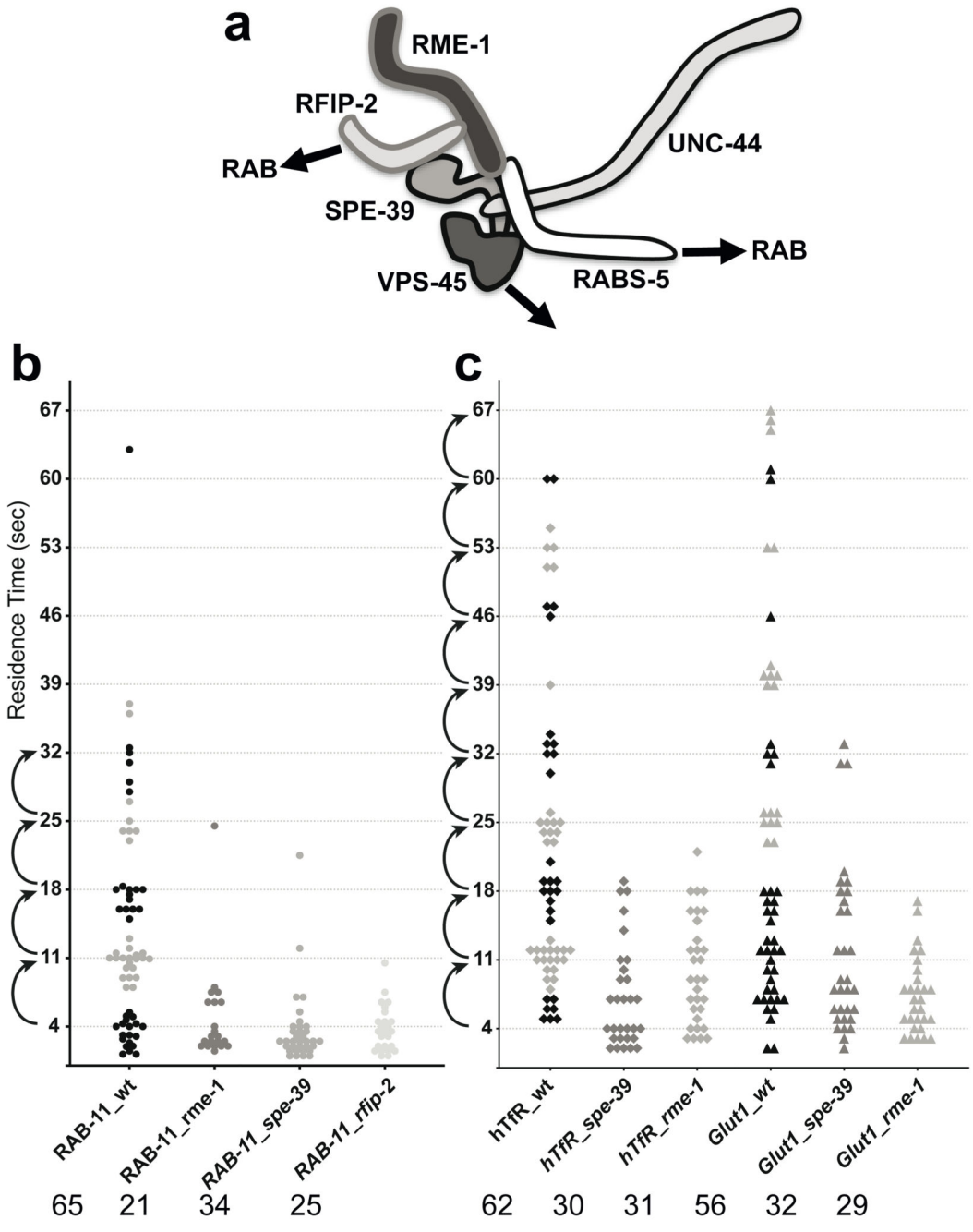

Extended Data Fig. 9. Kiss-and-run at sorting endosomes is quantal.

(a) Schematic drawing of the C. elegans FERARI tether. The Rab interaction modules RFIP-2 and RABS-5 are highlighted. (b) Quantification of GFP-RAB-11 vesicle residence times. Residence times occur in groups with an approximate 7 s -interval. The longer residence times are abolished in FERARI knock-downs. (c) Quantification of residence times of cargo vesicles containing hTfR-GFP and Glut1-GFP. The quantal distribution of residence times is similar to RAB-11 vesicles and longer residence times are abolished in FERARI RNAi conditions. Numbers of vesicles analyzed are indicated. See Statistical Source Data Extended Data 9.

Europe PMC Funders Author Manuscripts

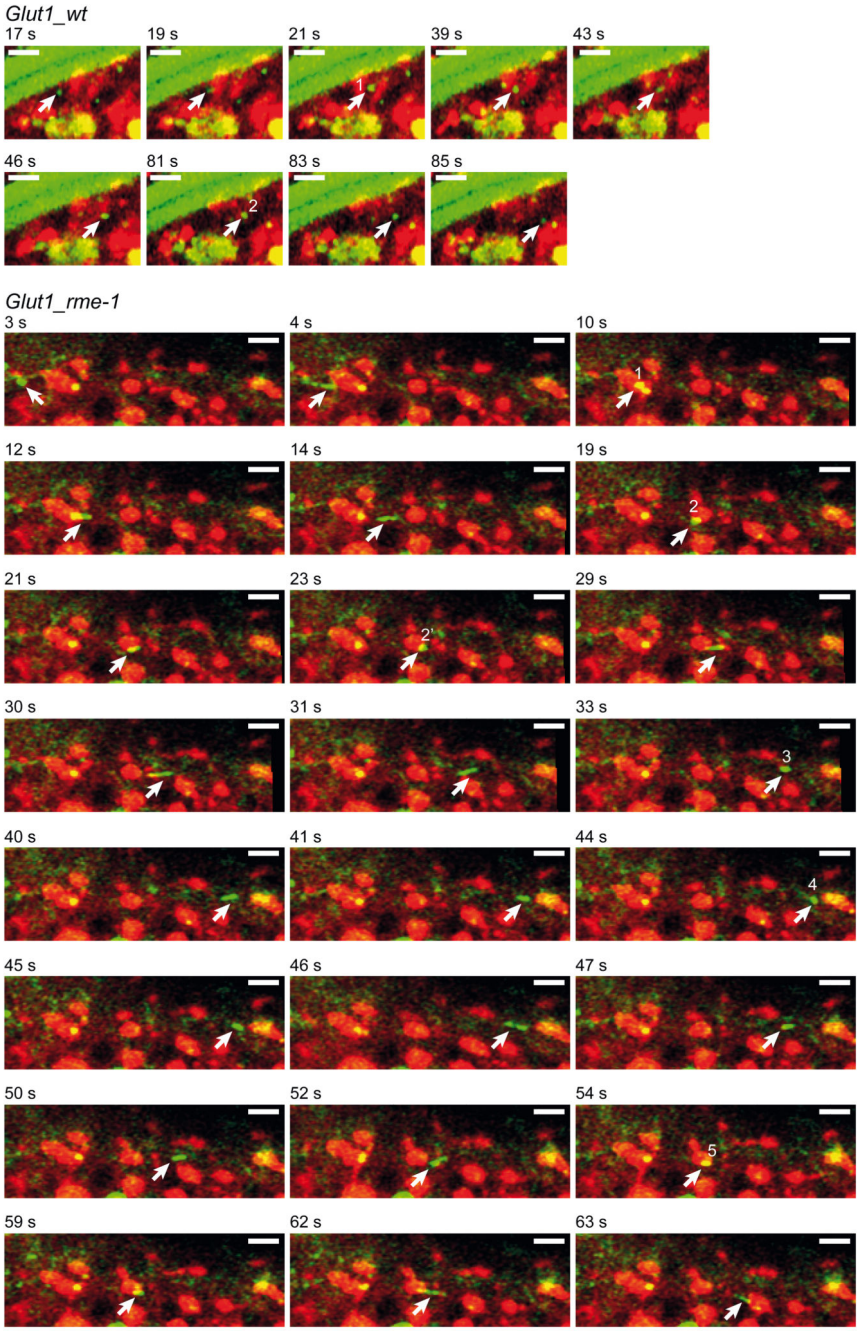

Extended Data Fig. 10. Glut1-GFP vesicle dynamics.

Movie stills showing Glut1-GFP vesicles docking to and pinching off from mCherry-SNX-1 compartments in mock-treated and *rme-1(RNAi)* worms. (see also movies S20 and S21). n=56 for *GLUT1_wt*, n=29 for *GLUT1_rme-1*. n represents number of vesicles. Scale bars: 2 μm.

Supplementary Material

Refer to Web version on PubMed Central for supplementary material.

Europe PMC Funders Author Manuscripts

Acknowledgements

We wish to thank Sheuli Begum and Jonas Fürst for excellent technical assistance with some of the experiments. The proteomics analysis was performed in the Proteomics Core Facility of the Biozentrum with the help of Suzette Moes and Paul Jenö. The Imaging Core Facility of the Biozentrum facilitated the generation of movies and in particular Laurent Guérard provided support for image analysis. Cells were sorted in the FACS Core Facility of the Biozentrum. We are grateful to Ian G. Macara for critical comments on the manuscript. Barth Grant and Pingsheng Liu are acknowledged for sharing strains. Some strains were provided by the CGC, which is funded by the NIH Office for Research Infrastructure Programs (P40 OG010440). This work was supported by the Swiss National Science Foundation (CRSII3_141956, 31003A_141207) and the University of Basel.

Data availability

The Source Data is for Fig. 1, 2, 3 (unprocessed blots), Fig. 1, 2, 3, 4, 5, 6, 7 (statistical source data), Extended Data 1, 2, 3, 4, 5, 7, 8 and Extended Data 1, 2, 3, 4, 5, 6, 7, 9 (statistical source data) have been provided in Source Data files. All other data supporting the findings of this study are available from the corresponding author on reasonable request.

References

1. Aflatounian M, et al. Novel VIPAS39 mutation in a syndromic patient with arthrogryposis, renal tubular dysfunction and intrahepatic cholestasis. Eur J Med Genet. 2016; 59: 237–239. [PubMed: 26808426]
2. Buggia-Prevot V, et al. A function for EHD family proteins in unidirectional retrograde dendritic transport of BACE1 and Alzheimer's disease Abeta production. Cell Rep. 2013; 5: 1552–1563. DOI: 10.1016/j.celrep.2013.12.006 [PubMed: 24373286]
3. Chen CH, Lo RW, Urban D, Pluthero FG, Kahr WH. alpha-granule biogenesis: from disease to discovery. Platelets. 2017; 28: 147–154. [PubMed: 28277061]
4. Haider NB, et al. Evaluation and molecular characterization of EHD1, a candidate gene for Bardet-Biedl syndrome 1 (BBS1). Gene. 1999; 240: 227–232. [PubMed: 10564830]
5. Link DC. SNAREing a new cause of neutropeni. Blood. 2013; 121: 4969–4970. [PubMed: 23788021]
6. Mellman I, Yarden Y. Endocytosis and cancer. Cold Spring Harb Perspect Biol. 2013; 5 a016949 doi: 10.1101/cshperspect.a016949 [PubMed: 24296170]
7. Meng Q, et al. Increased Expression of Eps15 Homology Domain 1 is Associated with Poor Prognosis in Resected Small Cell Lung Cancer. J Cancer. 2015; 6: 990–995. DOI: 10.7150/jca.11650 [PubMed: 26366212]
8. Tong D, et al. Increased Eps15 homology domain 1 and RAB11FIP3 expression regulate breast cancer progression via promoting epithelial growth factor receptor recycling. Tumour Biol. 2017; 39 1010428317691010 [PubMed: 28215104]
9. Chu CEL, Tang BL. Rab 10-a traffic controller in multiple cellular pathways and locations. J Cell Physiol. 2018; 233: 6483–6494. [PubMed: 29377137]
10. Wandinger-Ness A, Zerial M. Rab proteins and the compartmentalization of the endosomal system. Cold Spring Harb Perspect Biol. 2014; 6 a022616 doi: 10.1101/cshperspect.a022616 [PubMed: 25341920]
11. Solinger JA, Poteryaev D, Spang A. Application of RNAi technology and fluorescent protein markers to study membrane traffic in C. elegans. Methods Mol Biol. 2014; 1174: 329–347. [PubMed: 24947393]
12. Solinger JA, Spang A. Loss of the Sec1/Munc18-family proteins VPS-33.2 and VPS-33.1 bypasses a block in endosome maturation in Caenorhabditis elegans. Mol Biol Cell. 2014; 25: 3909–3925. DOI: 10.1091/mbc.E13-12-0710 [PubMed: 25273556]
13. Grant B, et al. Evidence that RME-1, a conserved C. elegans EH-domain protein, functions in endocytic recycling. Nat Cell Biol. 2001; 3: 573–579. [PubMed: 11389442]

14. Daumke O, et al. Architectural and mechanistic insights into an EHD ATPase involved in membrane remodelling. Nature. 2007; 449: 923–927. [PubMed: 17914359]
15. Melo A, et al. Structural insights into the activation mechanism of dynamin-like EHD ATPases. Proc Natl Acad Sci U S. 2017; 114: 5629–5634. DOI: 10.1073/pnas.1614075114 [PubMed: 28228524]
16. Pant S, et al. AMPH-1/Amphiphysin/Bin1 functions with RME-1/Ehd1 in endocytic recycling. Nat Cell Biol. 2009; 11: 1399–1410. DOI: 10.1038/ncb1986 [PubMed: 19915558]
17. Bonifacino JS, Rojas R. Retrograde transport from endosomes to the trans-Golgi network. Nat Rev Mol Cell Biol. 2006; 7: 568–579. [PubMed: 16936697]
18. Naslavsky N, Rahajeng J, Sharm M, Jovic M, Caplan S. Interactions between EHD proteins and Rab11-FIP2: a role for EHD3 in early endosomal transport. Mol Biol Cell. 2006; 17: 163–177. DOI: 10.1091/mbc.E05-05-0466 [PubMed: 16251358]
19. Traer CJ, et al. SNX4 coordinates endosomal sorting of TfnR with dynein-mediated transport into the endocytic recycling compartment. Nat Cell Biol. 2007; 9: 1370–1380. [PubMed: 17994011]
20. van Weering JR, Verkade P, Cullen PJ. SNX-BAR-mediated endosome tubulation is co-ordinated with endosome maturation. Traffic. 2012; 13: 94–107. [PubMed: 21973056]
21. Naslavsky N, Boehm M, Backlund PS Jr, Caplan S. Rabenosyn-5 and EHD1 interact and sequentially regulate protein recycling to the plasma membrane. Mol Biol Cell. 2004; 15: 2410–2422. DOI: 10.1091/mbc.E03-10-0733 [PubMed: 15020713]
22. Peplowsk K, Markgraf DF, Ostrowicz CW, Bange G, Ungermann C. The CORVET tethering complex interacts with the yeast Rab5 homolog Vps21 and is involved in endo-lysosomal biogenesis. Dev Cell. 2007; 12: 739–750. [PubMed: 17488625]
23. Plemel RL, et al. Subunit organization and Rab interactions of Vps-C protein complexes that control endolysosomal membrane traffic. Mol Biol Cell. 2011; 22: 1353–1363. DOI: 10.1091/mbc.E10-03-0260 [PubMed: 21325627]
24. Solinger JA, Spang A. Tethering complexes in the endocytic pathway: CORVET and HOPS. FEBS J. 2013; 280: 2743–2757. [PubMed: 23351085]
25. Ungermann C, Price A, Wickner W. A new role for a SNARE protein as a regulator of the Ypt7/Rab-dependent stage of docking. Proc Natl Acad Sci U S. 2000; 97: 8889–8891. DOI: 10.1073/pnas.160269997 [PubMed: 10908678]
26. Rahajeng J, Caplan S, Naslavsky N. Common and distinct roles for the binding partners Rabenosyn-5 and Vps45 in the regulation of endocytic trafficking in mammalian cells. Exp Cell Res. 2010; 316: 859–874. DOI: 10.1016/j.yexcr.2009.11.007 [PubMed: 19931244]
27. Spang A. Membrane Tethering Complexes in the Endosomal System. Front Cell Dev Biol. 2016; 4: 35. doi: 10.3389/fcell.2016.00035 [PubMed: 27243003]
28. Rogerson C, Gissen P. VPS33B and VIPAR are essential for epidermal lamellar body biogenesis and function. Biochim Biophys Acta Mol Basis Dis. 2018; 1864: 1609–1621. DOI: 10.1016/j.bbadis.2018.01.028 [PubMed: 29409756]
29. Gengyo-Ando K, et al. The SM protein VPS-45 is required for RAB-5-dependent endocytic transport in Caenorhabditis elegans. EMBO Rep. 2007; 8: 152–157. DOI: 10.1038/sj.embor.7400882 [PubMed: 17235359]
30. Nielsen E, et al. Rabenosyn-5, a novel Rab5 effector, is complexed with hVPS45 and recruited to endosomes through a FYVE finger domain. J Cell Biol. 2000; 151: 601–612. DOI: 10.1083/jcb.151.3.601 [PubMed: 11062261]
31. Guilherme A, et al. EHD2 and the novel EH domain binding protein EHBP1 couple endocytosis to the actin cytoskeleton. J Biol Chem. 2004; 279: 10593–10605. [PubMed: 14676205]
32. Lin SX, Grant B, Hirsh D, Maxfield FR. Rme-1 regulates the distribution and function of the endocytic recycling compartment in mammalian cells. Nat Cell Biol. 2001; 3: 567–572. [PubMed: 11389441]
33. Ackem KB, Sauder U, Solinger JA, Spang A. The ArfGEF GBF-1 Is Required for ER Structure, Secretion and Endocytic Transport in C. elegans. PLoS One. 2013; 8 e67076 doi: 10.1371/journal.pone.0067076 [PubMed: 23840591]
34. Chen CC, et al. RAB-10 is required for endocytic recycling in the Caenorhabditis elegans intestine. Mol Biol Cell. 2006; 17: 1286–1297. DOI: 10.1091/mbc.E05-08-0787 [PubMed: 16394106]

35. Sato K, Norris A, Sato M, Grant BDC. elegans as a model for membrane traffic. WormBook. 2014; 1–47. DOI: 10.1895/wormbook.1.77.2 [PubMed: 24778088]
36. Winter JF, et al. Caenorhabditis elegans screen reveals role of PAR-5 in RAB-11-recycling endosome positioning and apicobasal cell polarity. Nat Cell Biol. 2012; 14: 666–676. [PubMed: 22634595]
37. Sato M, Grant BD, Harad A, Sato K. Rab11 is required for synchronous secretion of chondroitin proteoglycans after fertilization in Caenorhabditis elegans. J Cell Sci. 2008; 121: 3177–3186. [PubMed: 18765566]
38. Shi A, et al. RAB-10-GTPase-mediated regulation of endosomal phosphatidylinositol-4,5-bisphosphate. Proc Natl Acad Sci U S. 2012; 109: E2306–2315. DOI: 10.1073/pnas.1205278109 [PubMed: 22869721]
39. Nordmann M, et al. The Mon1-Ccz1 complex is the GEF of the late endosomal Rab7 homolog Ypt7. Curr Biol. 2010; 20: 1654–1659. [PubMed: 20797862]
40. Poteryaev D, Datt S, Ackem K, Zerial M, Spang A. Identification of the switch in early-to-late endosome transition. Cell. 2010; 141: 497–508. [PubMed: 20434987]
41. Poteryaev D, Fares H, Bowerman B, Spang A. Caenorhabditis elegans SAND-1 is essential for RAB-7 function in endosomal traffic. EMBO J. 2007; 26: 301–312. DOI: 10.1038/sj.emboj.7601498 [PubMed: 17203072]
42. Gokool S, Tattersall D, Seaman MN. EHD1 interacts with retromer to stabilize SNX1 tubules and facilitate endosome-to-Golgi retrieval. Traffic. 2007; 8: 1873–1886. [PubMed: 17868075]
43. Shi A, et al. Regulation of endosomal clathrin and retromer-mediated endosome to Golgi retrograde transport by the J-domain protein RME-8. EMBO J. 2009; 28: 3290–3302. DOI: 10.1038/emboj.2009.272 [PubMed: 19763082]
44. Zhang Y, Grant B, Hirsh D. RME-8, a conserved J-domain protein, is required for endocytosis in Caenorhabditis elegans. Mol Biol Cell. 2001; 12: 2011–2021. DOI: 10.1091/mbc.12.7.2011 [PubMed: 11451999]
45. Diefenbacher M, Thorsteinsdottir H, Spang A. The Dsl1 tethering complex actively participates in soluble NSF (N-ethylmaleimide-sensitive factor) attachment protein receptor (SNARE) complex assembly at the endoplasmic reticulum in Saccharomyces cerevisiae. J Biol Chem. 2011; 286: 25027–25038. DOI: 10.1074/jbc.M110.215657 [PubMed: 21482823]
46. Zick M, Wickner W. The tethering complex HOPS catalyzes assembly of the soluble SNARE Vam7 into fusogenic trans-SNARE complexes. Mol Biol Cell. 2013; 24: 3746–3753. DOI: 10.1091/mbc.E13-07-0419 [PubMed: 24088569]
47. Campelo F, Fabrikant G, McMahon HT, Kozlov MM. Modeling membrane shaping by proteins: focus on EHD2 and N-BAR domains. FEBS Lett. 2010; 584: 1830–1839. [PubMed: 19836393]
48. Henkel AW, Almers W. Fast steps in exocytosis and endocytosis studied by capacitance measurements in endocrine cells. Curr Opin Neurobiol. 1996; 6: 350–357. [PubMed: 8794084]
49. Ryan T. Kiss-and-run, fuse-pinch-and-linger, fuse-and-collapse: the life and times of a neurosecretory granule. Proc Natl Acad Sci U S. 2003; 100: 2171–2173. DOI: 10.1073/pnas.0530260100 [PubMed: 12606723]
50. Rotem-Yehudar R, Galperin E, Horowitz M. Association of insulin-like growth factor 1 receptor with EHD1 and SNAP29. J Biol Chem. 2001; 276: 33054–33060. [PubMed: 11423532]
51. Lu Q, et al. Early steps in primary cilium assembly require EHD1/EHD3-dependent ciliary vesicle formation. Nat Cell Biol. 2015; 17: 228–240. [PubMed: 25686250]
52. Bem D, et al. VPS33B regulates protein sorting into and maturation of alpha-granule progenitor organelles in mouse megakaryocytes. Blood. 2015; 126: 133–143. DOI: 10.1182/blood-2014-12-614677 [PubMed: 25947942]
53. Brenner S. The genetics of Caenorhabditis elegans. Genetics. 1974; 77: 71–94. [PubMed: 4366476]
54. Solinger JA, Poteryaev D, Spang A. Application of RNAi technology and fluorescent protein markers to study membrane traffic in C. elegans. Methods Mol Biol. 2014; 1174: 329–347. [PubMed: 24947393]
55. Beuret N, et al. Amyloid-like aggregation of provasopressin in diabetes insipidus and secretory granule sorting. BMC biology. 2017; 15: 5. doi: 10.1186/s12915-017-0347-9 [PubMed: 28122547]

56. Wartosch L, Gunesdogan U, Graham SC, Luzio JP. Recruitment of VPS33A to HOPS by VPS16 Is Required for Lysosome Fusion with Endosomes and Autophagosomes. Traffic. 2015; 16: 727–742. DOI: 10.1111/tra.12283 [PubMed: 25783203]

57. Hsu F, Hu F, Mao Y. Spatiotemporal control of phosphatidylinositol 4-phosphate by Sac2 regulates endocytic recycling. The Journal of cell biology. 2015; 209: 97–110. DOI: 10.1083/jcb.201408027 [PubMed: 25869669]

58. Schindelin J, et al. Fiji: an open-source platform for biological-image analysis. Nature methods. 2012; 9: 676–682. DOI: 10.1038/nmeth.2019 [PubMed: 22743772]

59. Legland D, Arganda-Carreras I, Andrey P. MorphoLibJ: integrated library and plugins for mathematical morphology with ImageJ. Bioinformatics (Oxford, England). 2016; 32: 3532–3534. [PubMed: 27412086]

60. Tinevez JY, et al. TrackMate: An open and extensible platform for single-particle tracking. Methods (San Diego, Calif). 2017; 115: 80–90. [PubMed: 27713081]

61. Gul-Mohammed J, Arganda-Carreras I, Andrey P, Galy V, Boudier T. A generic classification-based method for segmentation of nuclei in 3D images of early embryos. BMC bioinformatics. 2014; 15: 9. doi: 10.1186/1471-2105-15-9 [PubMed: 24423252]

62. Ollion J, Cochennec J, Loll F, Escude C, Boudier T. TANGO: a generic tool for high-throughput 3D image analysis for studying nuclear organization. Bioinformatics (Oxford, England). 2013; 29: 1840–1841. DOI: 10.1093/bioinformatics/btt276 [PubMed: 23681123]

Europe PMC Funders Author Manuscripts

Europe PMC Funders Author Manuscripts

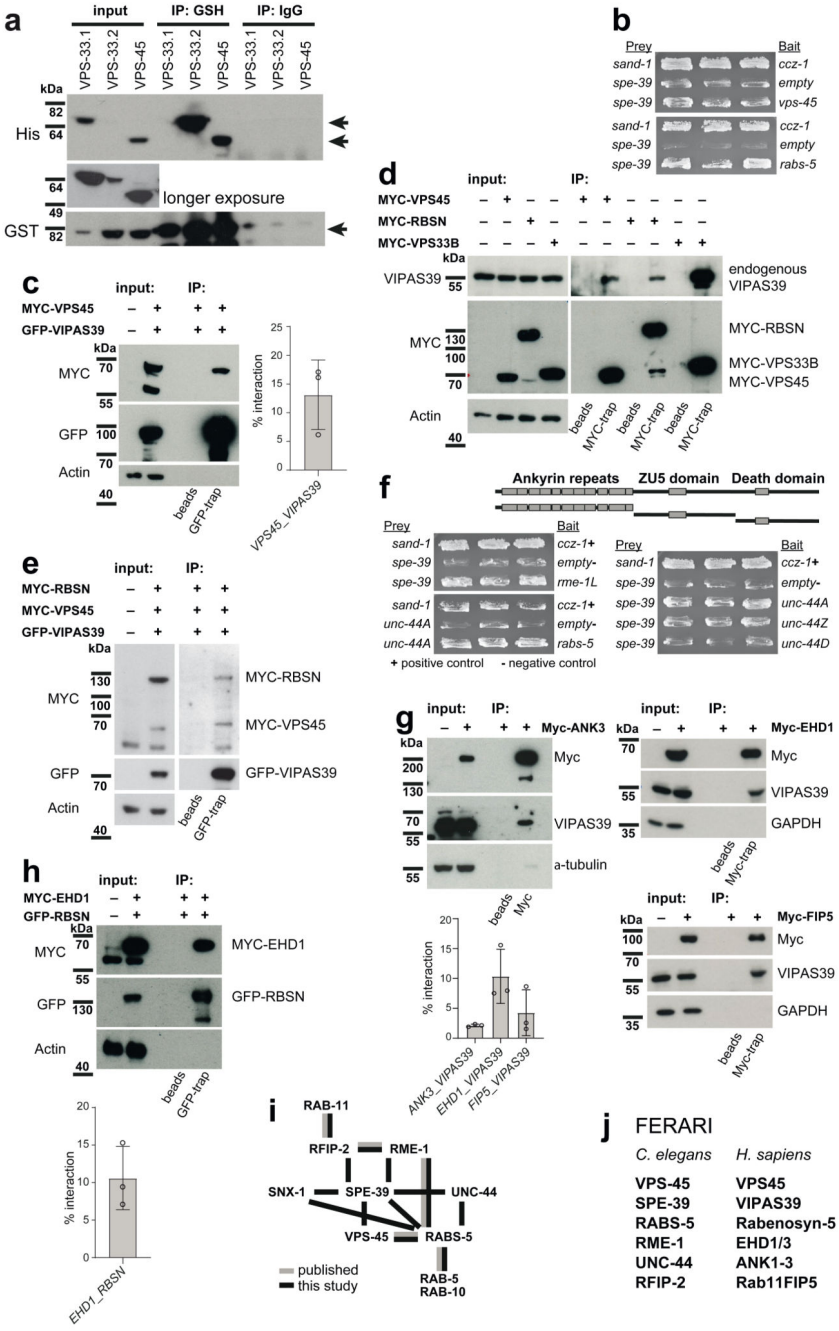

Figure 1. Conserved interactions between FERARI components

(a) Recombinant SPE-39 protein from *E. coli* interacts with VPS-45. SPE-39-GST was co-expressed with VPS-33.1, VPS-33.2 or VPS-45. Pull-downs were performed with either GSH-or IgG-beads as indicated. n=3 biologically independent experiments. For quantification see Extended Data 3d. (b) Yeast two hybrid assays show interactions between SPE-39 and VPS-45 as well as SPE-39 and RABS-5. n=3 biologically independent yeast transformants were grown on plates with galactose but lacking leucine; experiment was performed n= 6. The interaction between SAND-1 and CCZ-1 was used as positive

control, empty vector of activation domain plasmid pJG4-5 as negative control. (c) Interaction between VIPAS39 to VPS45 in HEK-293 cells. Cells were co-transfected with myc-tagged VPS45 and GFP-tagged VIPAS39. Co-immunoprecipitation with either control or GFP-trap beads. Protein were detected with antibodies against myc, GFP and actin. n=3 independent experiments. Quantification of interaction show the mean ± s.d. (d) Interaction of endogenous VIPAS39 with rabenosyn-5 and VPS45. Co-immunoprecitation of myc-tagged Rabenosyn-5, VPS45, or VPS33B. VIPAS39, myc and actin were detected. Interaction between VIPAS39 and VPS33B served as a positive control. n=3 independent experiments. (e) Interaction of VIPAS39, VPS45 and rabenosyn-5 in triple transfected cells. myc-Rabenosyn-5 and myc-VPS45 were co-immunoprecitipated with GFP-VIPAS39. n= 3 independent experiments (f) Yeast two hybrid interactions between SPE-39 and RME-1, UNC-44, as well as between UNC-44 and RABS-5. UNC-44 was subcloned into three domains as indicated in the schematic drawing. n=3 biologically independent yeast transformants; experiment was performed n= 6. (g) Binding of FERARI components to endogenous VIPAS39. Myc-ANK3, Myc-EHD1 or myc-RAB11FIP5 were immunoprecipitated with myc- or control-beads as indicated. n=3 independent experiments. Quantification displays mean ± s.d. (h) Co-immunoprecipitation of myc-EHD1 and GFP-Rabenosyn-5. n=3 independent experiments. Quantification of interaction shows the mean ± s.d. (i) Summary of interactions between FERARI components. (j) Table of FERARI components in *C. elegans* and humans. See Unprocessed Blots Figure 1 and Statistical Source Data Figure 1.

Europe PMC Funders Author Manuscripts

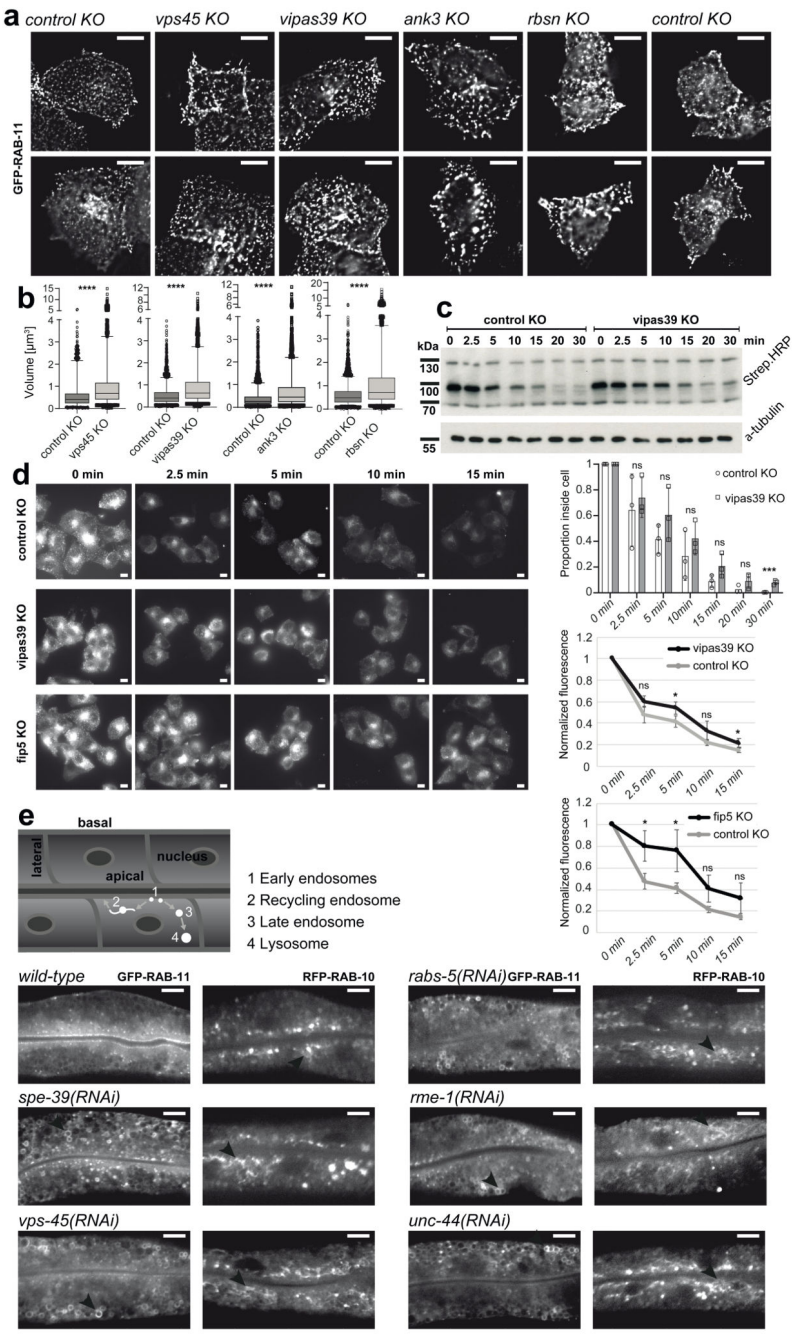

Figure 2. Loss of FERARI affects endosomal recycling

(a) Knock-out of vipas39, vps45, rbsn and ank3 cause enlargement of Rab11 compartments in HeLa cells. Representative images from live cell imaging of Rab11-GFP in control and KO cells. Scale bars: 10 µm. n=3 independent experiments. (b) Quantification of deconvolved and FIJI processed images shown in (a). Volume units [μm^3] were determined. For ctr ko, vipas39 ko and vps45 ko total n= 6,075; 6,104; and 6,062 rab11 positive vesicles were counted; for ctr ko and ank3 ko total n=6,081 and n=6,056 vesicles; for ctr ko and rbsn ko total n=6,048 vesicles and n=6,067 vesicles. >2,000 vesicles from each

replicate (n=3 independent experiments) were analyzed. Box Plot: box 25-75 percentile with median; whiskers: 5-95 percentile (P=<0.0001). are depicted. (c) Tfn recycling is reduced in vipas39 KO cells. Pulse-chase experiment with Tfn-Biotin. Internal Tfn-Biotin was detected with Streptavidin HRP. n=3 independent experiments (Data show the mean ± s.d). 2.5 min: P=0.6288; 5 min: P=0.2351; 10 min: P=0.3571; 15 min: P=0.1233; 20 min: P=0.1445; 30 min: P=0.0014. (d) Tfn-Alexa594 recycling is reduced in ferari KO cells. Pulse chase experiment. Scale bars: 10 μm. For quantification at t=0: ctr n=153 cells; fip5 ko n=166 cells; vipas39 ko n=176 cells. At t=2.5 min: ctr n=161 cells; fip5 ko n= 165 cells (P=0.0234); vipas39 ko n=143 cells (P=0.0663) cells. At t=5 min: ctr n=152 cells; fip5 ko n=157 cells (P=0.0391); vipas39 ko n=162 cells (P=0.0420). At t=10 min: ctr n=148 cells; fip5 ko n= 149 cells (P=0.0612); vipas39 n= 151 cells (P=0.1129). At t=15 min: ctr n=146 cells; fip5 ko n= 152 cells (P=0.1031); vipas39 n= 150 cells (P=0.0418) from 3 biological replicates (> 40 cells/replicate). Data show the mean ± s.d. (e) GFP-RAB-11 and RFP-RAB-10 structures are affected by *FERARI(RNAi)*. Schematic representation of *C. elegans* intestinal cells with endosomal compartments. GFP-RAB-11 structures are enlarged and RFP-RAB-10 networks are grossly extended in *FERARI(RNAi)* animals. Arrowheads point towards aberrant structures. Scale bars: 10 μm. The mean ± standard deviation is shown; n=3 independent experiments (n=20 animals); *P < 0.05, **P < 0.01, ***P < 0.00, ****P < 0.0001 and n.s., P > 0.05. Two-tailed Student’s t-tests were used for all analyses. See Unprocessed Blots Figure 2 and Statistical Source Data Figure 2.

Europe PMC Funders Author Manuscripts

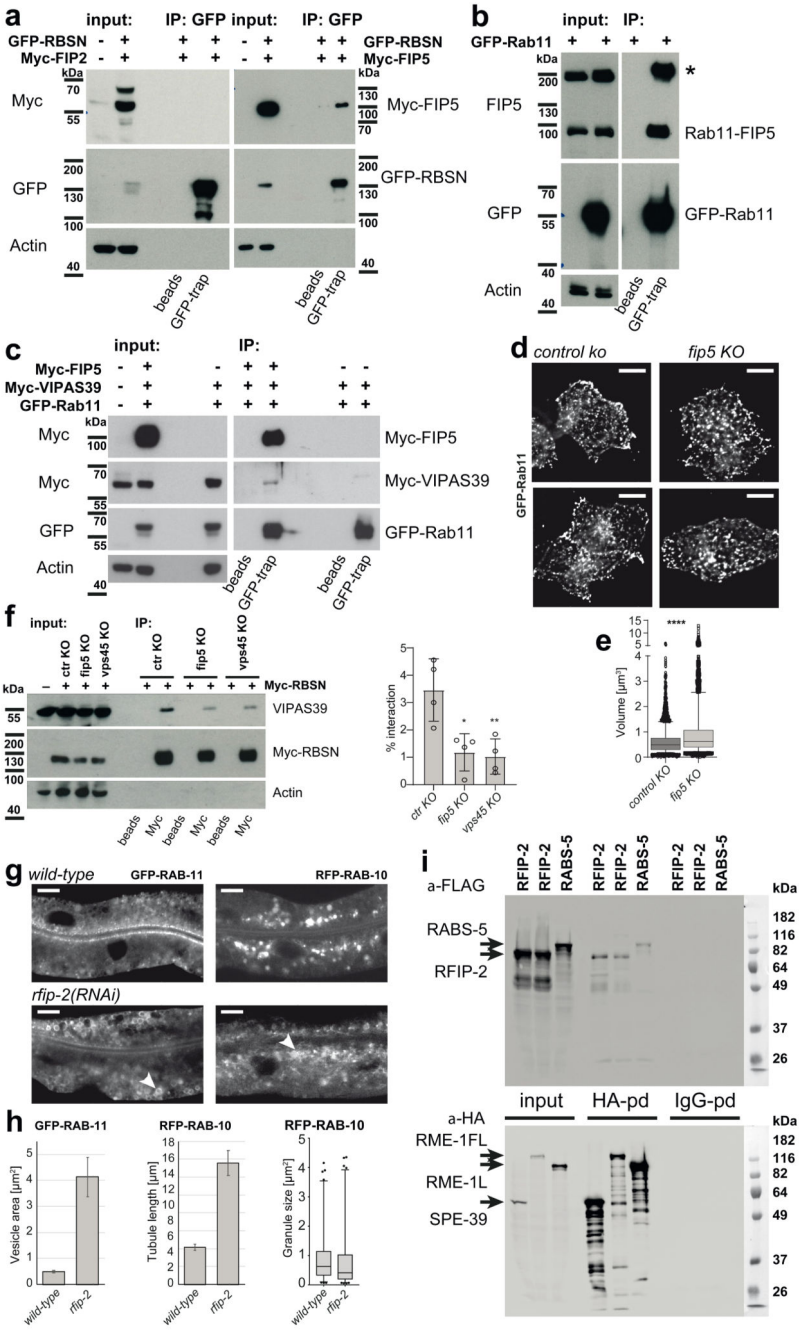

Figure 3. Rab11FIP5 is part of FERARI and provides the link to Rab11

(a) Rabenosyn-5 binds to Rab11FIP5 but not to Rab11FIP2. myc-tagged Rab11FIP5 but not Rab11FIP2 was co-immunoprecipitated with GFP-Rabenosyn-5. Representative images. n=3 independent experiments. Quantification in Extended Data 3E. (b) Western blot of immunoprecipitation of endogenous Rab11FIP5 with GFP-Rab11. n=3 independent experiments. Quantification in Extended Data 3F. (c) Rab11 binds to FERARI through Rab11FIP5. HEK-293 cells were co-transfected with GFP-Rab11 and myc-VIPAS39 in the presence or absence of myc-Rab11FIP5. n=3 independent experiments. (d) Live cell imaging

of GFP-Rab11 in fip5 KO HeLa cells. Scale bars: 10 μm. n=3 independent experiments. (e) Quantification of deconvolved and FIJI processed images shown in (d). GFP-Rab11 positive vesicles were counted in ctr (n=6,081) and fip5 ko (n=6,059) from n=3 independent biological replicates (>2,000 vesicles/replicate). Box plot: box represents 25-75 percentile with median; whiskers: 5-95 percentile (P=<0.0001). (f) Interaction between RBSN and endogenous VIPAS39 is reduced in fip5 and vps45 KO cells. ctr KO, rab11fip5 KO and vps45 KO HEK-293 cells were transfected with myc-RBSN. Immunoprecipitated proteins and inputs were probed with antibodies against myc, VIPAS39 and actin. Quantification of interactions of n=4 independent experiments Data show the mean ± s.d.; P=0.0141 (fip5 ko); P=0.0099 (vps45 ko). (g) Phenotypes of *rfip-2* knock-downs in worm intestinal cells expressing GFP-RAB-11or RFP-RAB-10. Arrowheads point to abnormal RAB-11 and RAB-10 compartments. n=3 independent RNAi experiments (n=20 animals). (h) Quantification of *rfip-2* phenotypes shown in (g). mean ± s.d. is shown. Box plot: box represents 25-75 percentile with median; whiskers 1-99 percentile. Scale bars: 10 μm. (i) Interactions between proteins in the yeast two hybrid vectors were tested biochemically with pull-downs. Worm RFIP-2 (Y39F10B.1) binds to RME-1 and SPE-39. Interaction between RME-1 and RABS-5 also occurs in worms. Quantification in Extended Data 3G. The mean values ± standard deviations are shown; n=3 independent experiments; *P < 0.05, **P < 0.01, ***P < 0.00, ****P < 0.0001 and n.s. P > 0.05. Two-tailed Student’s t-tests were used for all the analyses. See Unprocessed Blots Figure 3 and Statistical Source Data Figure 3.

Europe PMC Funders Author Manuscripts

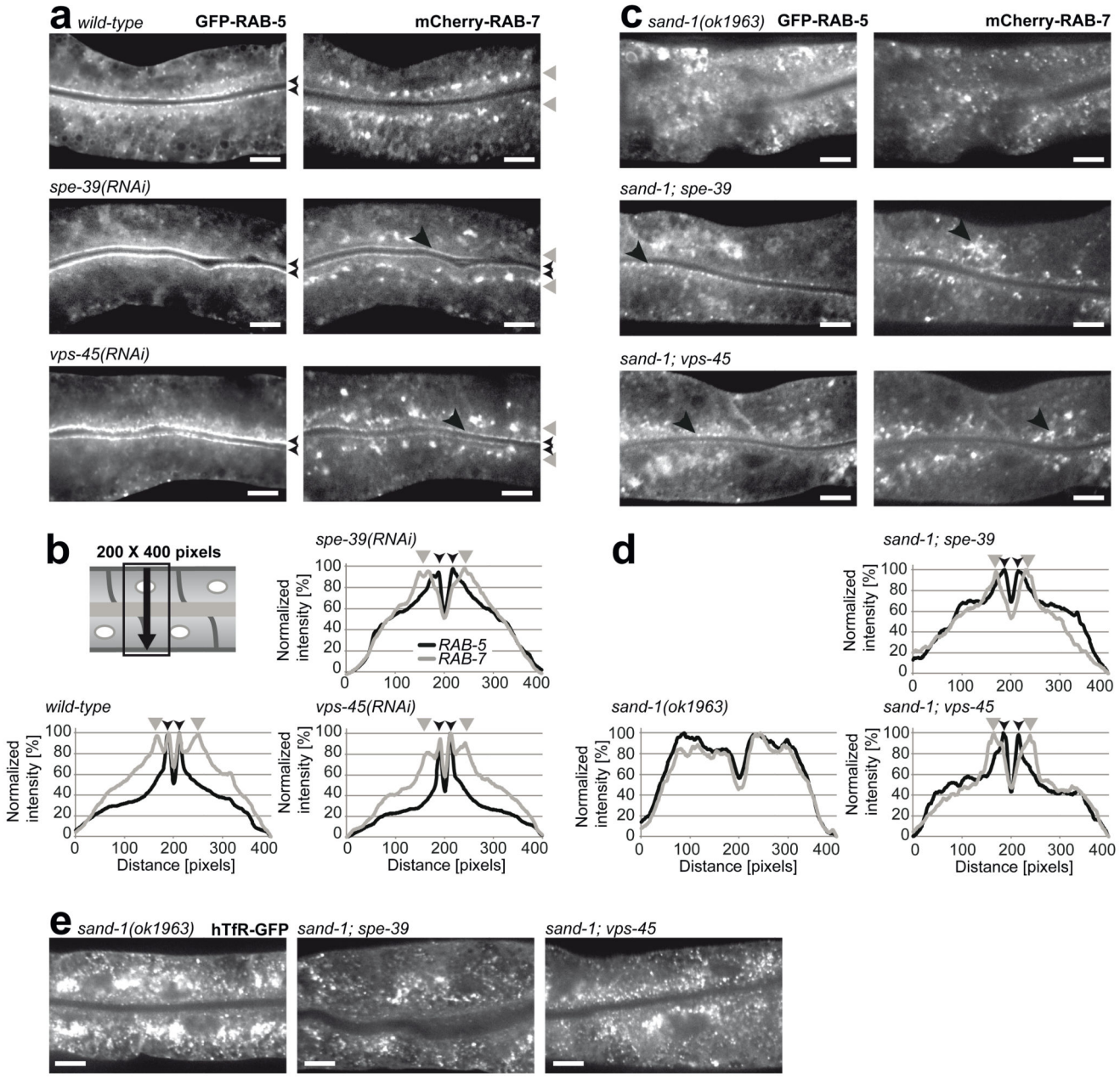

Figure 4. FERARI may act on sorting endosomes but is not essential for transport to lysosomes

(a) RAB-5 positive compartments are affected by *spe-39(RNAi)* and *vps-45(RNAi)*. GFP-RAB-5 signal remains confined to the apical membrane (small black arrowheads and these compartments even seem to mature to RAB-7 (large black arrowheads). General RAB-7 compartment is largely unaffected (gray arrowheads). n=3 independent RNAi experiments (n=20 animals). Scale bars: 10 μm. (b) Quantification of RAB-5 and RAB-7 phenotypes. Schematic representation of a worm gut and the area used for quantification (line plot with 200 pixels width). Small black arrowheads indicate RAB-5 peaks, gray arrowheads RAB-7 compartments. n=5 worms/curve. (c) Enlarged RAB-5 compartments in *sand-1(ok1963)* worms are partially restored in *spe-39* and *vps-45* knock-downs. The dispersed and

disorganized RAB-7 compartments of *sand-1(ok1963)* worms are also partially suppressed by loss of FERARI. Black arrowheads point to restored compartments. n=3 independent RNAi experiments (n=20 animals). Scale bars: 10 μm. (d) Quantification of *sand-1* suppression phenotypes as in (b). n=5 worms/curve. (e) In *sand-1(ok1963)* worms the degradation pathway is blocked and hTfR-GFP accumulates in very bright endosomes. The hTfR-GFP signal is reduced in *spe-39(RNAi)* and *vps-45(RNAi)*. n=3 independent RNAi experiments (n=20 animals). Scale bars: 10 μm. See Statistical Source Data Figure 4.

Europe PMC Funders Author Manuscripts

Europe PMC Funders Author Manuscripts

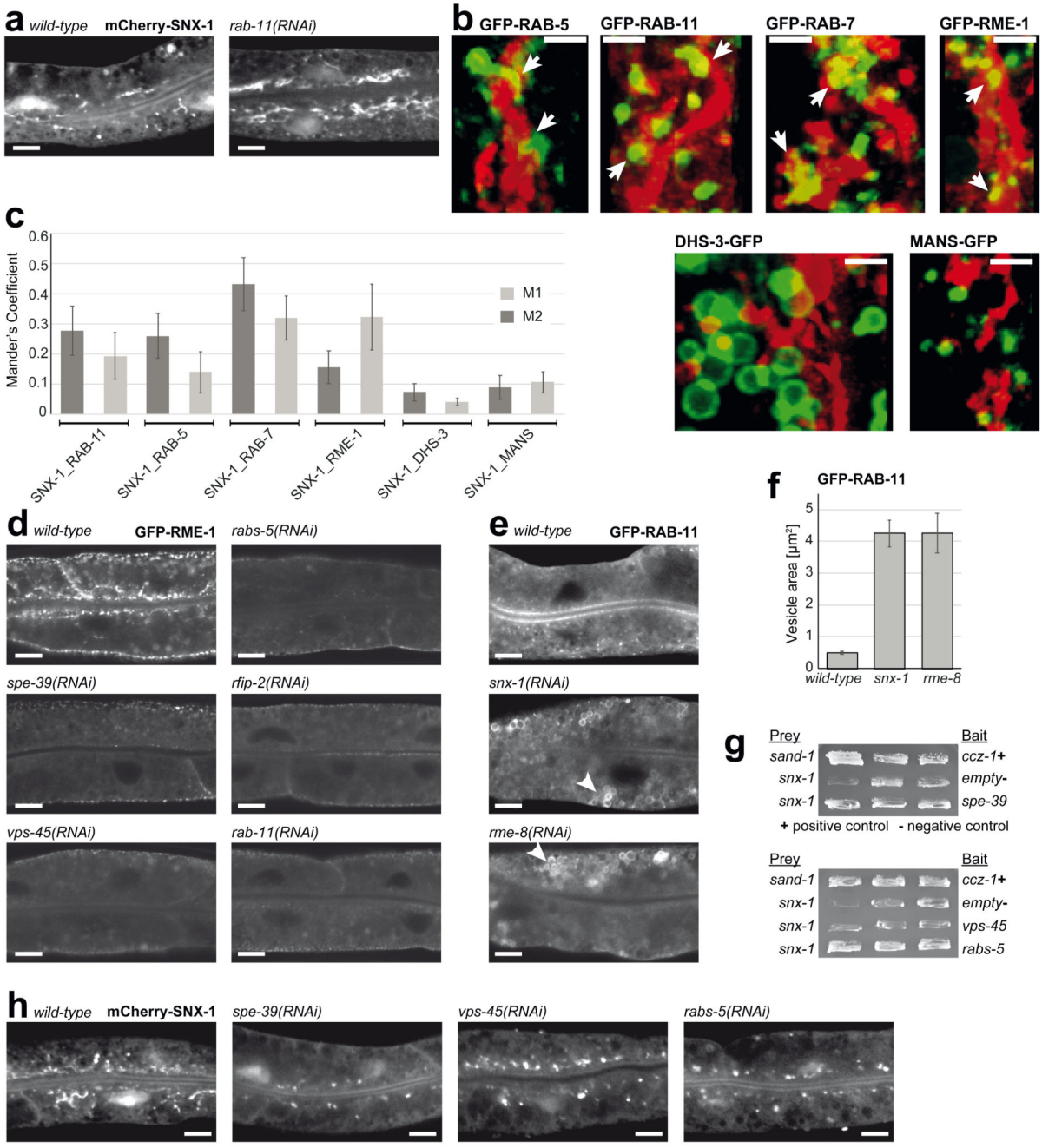

Figure 5. FERARI is present on and required for the maintenance of SNX-1 active recycling compartments in *C. elegans*

(a) mCherry-SNX-1 tubules are elongated and accumulate in *rab-11(RNAi)* worms. n= 3 independent RNAi experiments (n=20 animals). Scale bars: 10 µm. (b) mCherry-SNX-1 networks sometimes coincide with the position of RAB-11, RAB-5, RAB-7 and RME-1 compartments. Worms expressing mCherry-SNX-1 and either RAB-5, RAB-11, RAB-7 and RME-1 show some overlap between the networks and the globular compartments. White arrows point to sites of overlap. As controls DHS-3 (lipid droplets) and MANS (Golgi) were used. n=3 independent RNAi experiments (n=30 animals). Scale bars: 3 µm. (c)

Quantification of co-localization using Mander's coefficient. n=10 animals were measured. mean ± s.d. is indicated. (d) GFP-RME-1 localization is abolished in FERARI knock-downs *(spe-39, vps-45, rabs-5, rfip-2* and *rab-11*). n=3 independent RNAi experiments (n= 20 animals). Scale bars:10 μm. (e) Knock-down of *snx-1* and its interactor *rme-8* show FERARI-like RAB-11 phenotypes. Arrowheads point to enlarged RAB-11 compartments. n=3 independent RNAi experiments (n= 20 animals). Scale bars =10 μm. (f) Quantification of phenotypes shown in (e). n=10 vesicles each were measured in n= 6 animals; mean ± s.d. is indicated. (g) Yeast two hybrid interactions of FERARI subunits with SNX-1. n= 3 independent transformants were analyzed in n= 6 experiments. (h) Networks formed by mCherry-SNX-1 are lost in *spe-39(RNAi)*, *vps-45(RNAi)* and *rabs-5(RNAi)* intestinal cells. n=3 independent RNAi experiments (n=20 animals). Scale bars:10 μm. See Statistical Source Data Figure 5.

Europe PMC Funders Author Manuscripts

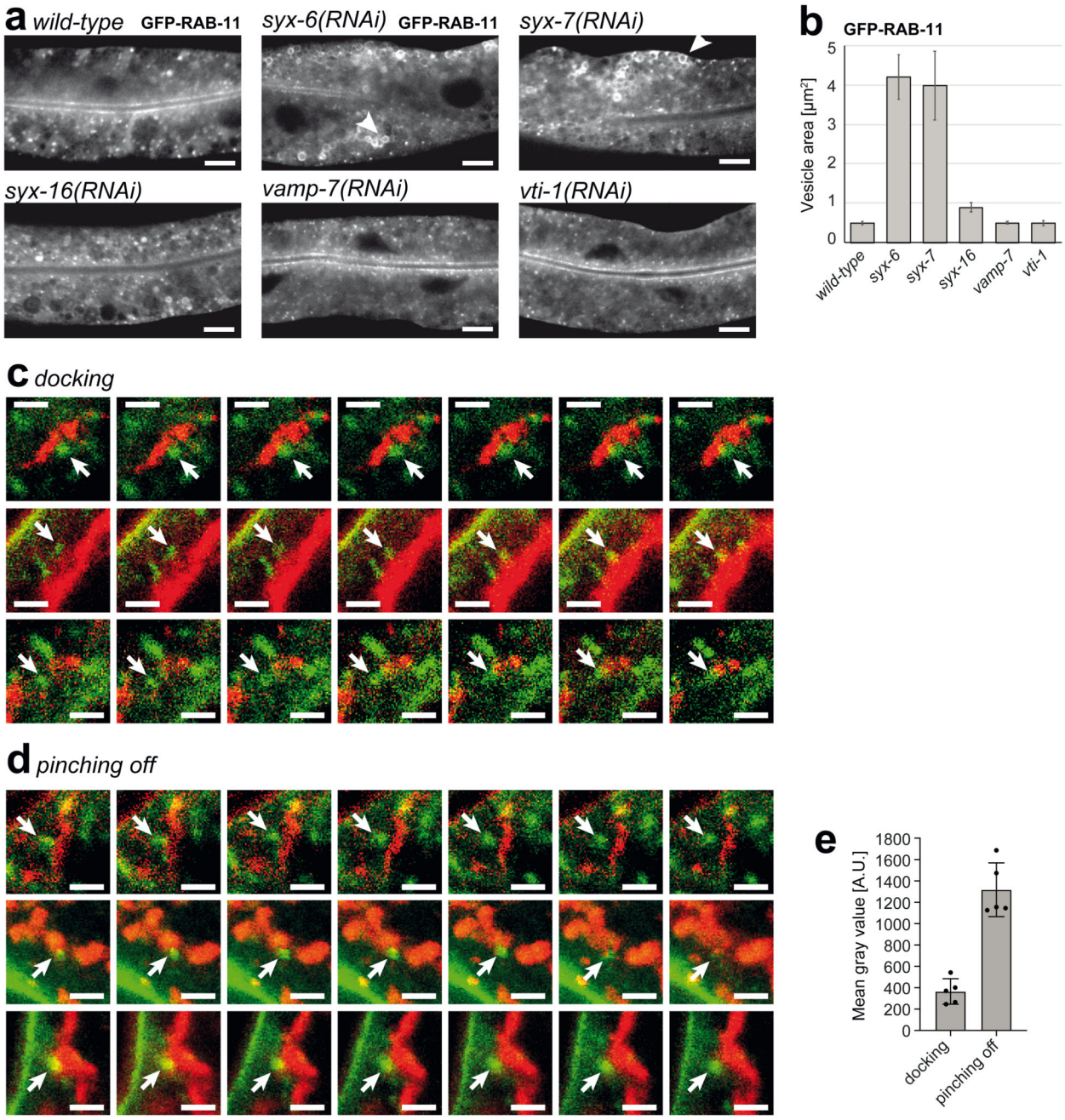

Figure 6. The SNAREs SYX-6 and SYX-7 act in the FERARI-dependent RAB-11 recycling pathway

(a) SNARE knock-downs show distinct phenotypes on RAB-11 compartments. While *syx-6* and *syx-7(RNAi)* show enlarged RAB-11 compartments (arrowheads), *syx-16, vamp-7* and *vti-1(RNAi)* had no effect. n=3 independent RNAi experiments (n= 20 animals). Scale bars: 10 µm. (b) Quantification of phenotypes shown in (a). n=10 structures for each of n=6 worms was measured; mean ± s.d. is indicated. (c) Stills from movies with GFP-RAB-11 and mCherry-SNX-1 compartments, showing docking of globular RAB-11 to SNX-1 tubules. Arrows point to RAB-11 compartment of interest. Please note the yellow

Europe PMC Funders Author Manuscripts

overlap in later pictures to the right. n=3 independent RNAi experiments (n=30 animals). Scale bars: 2 μm. (Movies S8-S10) (d) Stills from movies showing pinching off of RAB-11 globular compartments from SNX-1 tubules. Arrows point to RAB-11 compartment starting out with some overlap (yellow) and moving away from SNX-1 tubules. Time between stills is 30 sec (every 3rd image in movies). n=3 independent RNAi experiments (n= 30 animals). Scale bars: 2 μm. (Movies S11-S13) (e) Docking RAB-11 compartments are less bright than pinching off RAB-11 compartments. Brightness was measured over 10 frames of 5 movies each. n=5 movies were quantified; mean ± s.d. is indicated. See Statistical Source Data Figure 6.

Europe PMC Funders Author Manuscripts

Europe PMC Funders Author Manuscripts

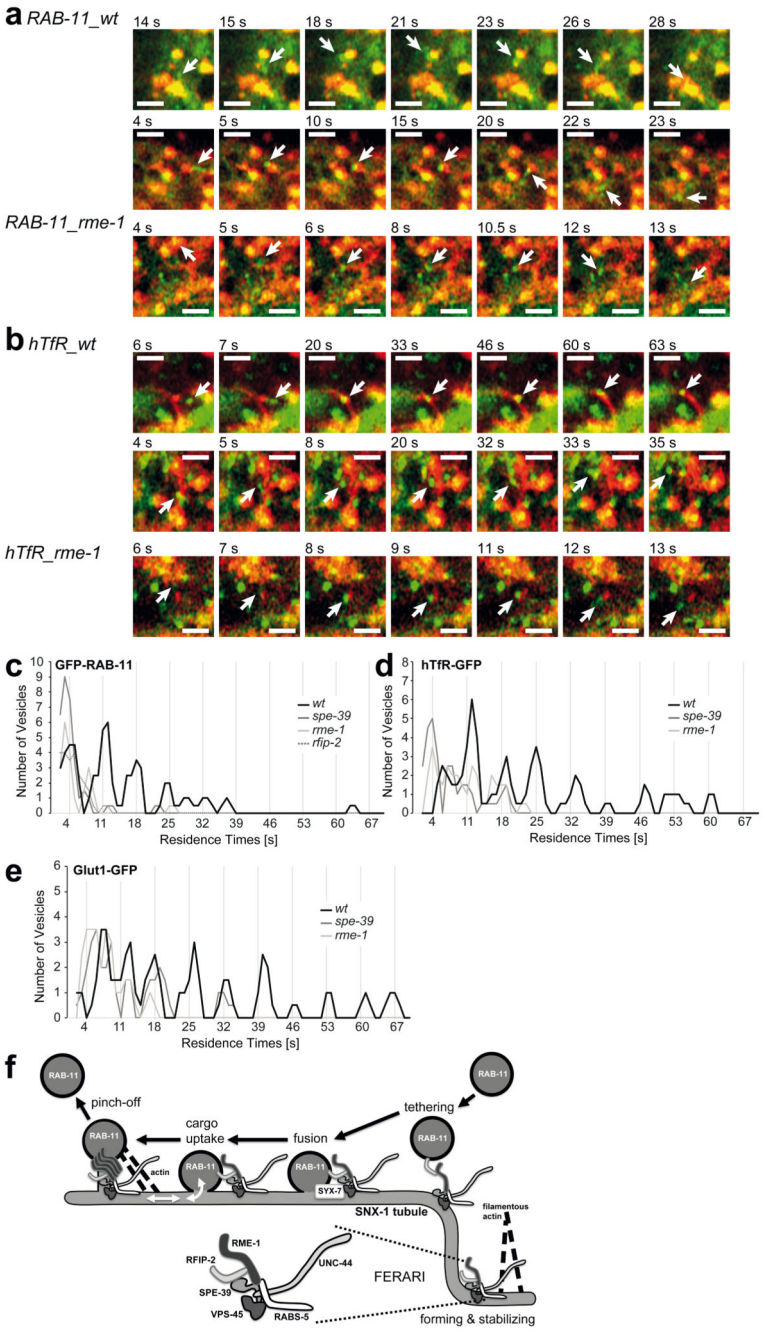

Figure 7. FERARI promotes kiss-and-run vesicle dynamics and quantal cargo uptake.

(a) Movie stills of GFP-RAB-11 vesicles docking and pinching off from mCherry-SNX-1 compartments in wt and *rme-1(RNAi)*. Times of frames are shown and arrows point to RAB-11 vesicles. n=3 independent experiments (n =30 animals). Scale bars: 2 μm. (Movies S14-S16) (b) hTfR-GFP vesicles behave in a similar way as RAB-11 vesicles. Shown are examples of hTfR vesicles in wt and *rme-1(RNAi)* worms (arrows). n=3 independent RNAi experiments (n=30 animals). Scale bars: 2 μm. (Movies S17-S20) (c)-(e) Binning of vesicles according to residence times (primary data in Extended Data 9B, C). The moving

average is calculated to highlight the peaks of residence times starting at approximately 4 sec and continuing at around 7- sec intervals. n=65 for *wild-type*, n=21 for *rme-1(RNAi)*, n=34 for *spe-39(RNAi)* and n=25 for *rfip-2(RNAi)* in (c), n= 62 for *wild-type*, n=30 for *spe-39(RNAi)* and n=31 for *rme-1(RNAi)* in (d), n=56 for *wild-type*, n=32 for *spe-39(RNAi)* and n=29 for *rme-1(RNAi)* in (e). (f) Model of FERARI recycling (see also movie S22). A putative structure of FERARI is shown below, based on interactions between the components and approximate size of proteins. Functions of FERARI might include forming and stabilizing SNX-1 sorting/recycling tubules. FERARI could tether RAB-11 compartments to these tubules, followed by membrane fusion through VPS-45 binding of the SNAREs SYX-6 and SYX-7. The RAB-11 compartment would be stabilized with an open pore to the SNX-1 tubule because of the presence of an RME-1 constriction ring. After sorting of cargo, the pinching activity of RME-1 - potentially coupled to UNC-44 interaction with actin - will allow the RAB-11 compartment to leave the sorting station. See Statistical Source Data Figure 7.

Europe PMC Funders Author Manuscripts